J. Fluid Mech. (2022), *vol*. 939, A25, doi:10.1017/jfm.2022.206

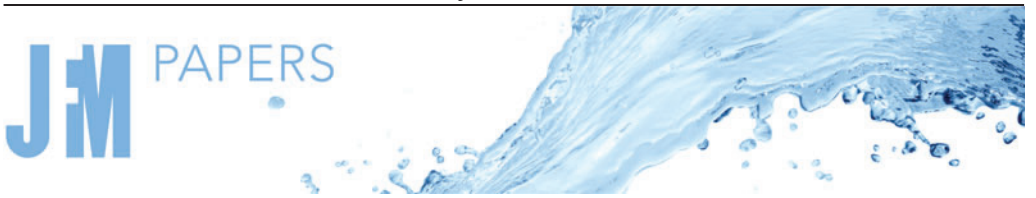

Non-homogeneous analysis of rogue wave probability evolution over a shoal

S. Mendes[1,2,†], **A. Scotti**[3], **M. Brunetti**[1,2] **and J. Kasparian**[1,2]

[1]Group of Applied Physics, University of Geneva, Chemin de Pinchat 22, 1227 Carouge, Switzerland

[2]Institute for Environmental Sciences, University of Geneva, Boulevard Carl-Vogt 66, 1205 Geneva, Switzerland

[3]Department of Marine Sciences, University of North Carolina at Chapel Hill, Chapel Hill, NC 27599, USA

(Received 28 May 2021; revised 10 January 2022; accepted 3 March 2022)

Non-equilibrium evolution of wave fields, as occurring over sudden bathymetry variations, can produce rogue seas with anomalous wave statistics. We handle this process by modifying the Rayleigh distribution through the energetics of second-order theory and a non-homogeneous reformulation of the Khintchine theorem. The resulting probability model reproduces the enhanced tail of the probability distribution of unidirectional wave tank experiments. It also describes why the peak of rogue wave probability appears atop the shoal, and explains the influence of depth on variations in peak intensity. Furthermore, we interpret rogue wave likelihoods in finite depth through the H–σ diagram, allowing a quick prediction for the effects of rapid depth change apart from the probability distribution.

Key words: surface gravity waves, coastal engineering

1. Introduction

Ocean statistics offers numerous applications, particularly in marine and offshore safety (Toffoli *et al.* 2005). Models for short- and long-term statistics of water waves are used to define the operating envelope for ocean vessels and fixed offshore structures, respectively. Furthermore, understanding the mechanisms of formation of rogue waves has received

† Email address for correspondence: saulo.dasilvamendes@unige.ch

a considerable amount of attention in past decades (Dysthe, Krogstad & Muller 2008; Onorato *et al.* 2013). Defined as waves at least twice as tall as the significant wave height (Haver 2000; Dysthe *et al.* 2008), rogue waves present a looming danger to offshore operations (Faulkner & Buckley 1997; Faukner 2002). Theories of rogue wave formation include the Benjamin and Feir instability (Benjamin & Feir 1967) arising in surface gravity waves, described by the nonlinear Schrödinger equation (Zakharov & Ostrovsky 2009; Onorato *et al.* 2013), and linear mechanisms such as constructive interference (Boccotti 2000; Fedele *et al.* 2016; Dematteis *et al.* 2019). From a statistical point of view, any particular theory relies on its ability to reproduce the tail of the wave amplitude probability distribution.

Longuet-Higgins (1952) applied methods and ideas from signal processing (Rice 1945) to oceanography (see St Denis & Pierson (1953) for a review). In particular, his approach took the underlying assumptions of Rice (1945) about homogeneity and ergodicity for granted. Therefore, the resulting non-dimensional Rayleigh distribution of wave heights cannot account for the varying sea state parameters, such as steepness (Stansell 2004) or depth (Glukhovskii 1966). The same limitation applies to higher-order analytical distributions (Karmpadakis, Swan & Christou 2020; Mendes, Scotti & Stansell 2021). Though these standard approaches have had considerable success in explaining the observed directional spectrum and wave properties (Phillips 1958; Hasselmann 1962; Pierson & Moskowitz 1964), the need for the ergodicity and spatial homogeneity assumptions essentially prevents the use of spectral analysis techniques in unsteady conditions or during isolated events, such as rogue waves (Donelan, Drennan & Magnusson 1996). Furthermore, Haver & Andersen (2000) were the first to suggest a link between rogue waves and non-stationarity. Nevertheless, we still lack a framework to account for unsteady conditions, such as shoaling. (For a review of the consequences of non-stationarity/homogeneity, see Appendix A.)

Following the laboratory experiments of Trulsen, Zeng & Gramstad (2012), considerable attention has been given to the shoaling effect on rogue wave formation. Waves approaching a sudden change in bathymetry provide an ideal configuration to probe out-of-equilibrium conditions (Trulsen 2018). Additional experiments (Raustøl 2014; Ma, Ma & Dong 2015; Bolles, Speer & Moore 2019; Zhang *et al.* 2019; Zou *et al.* 2019; Trulsen *et al.* 2020) and numerical studies (Zeng & Trulsen 2012; Gramstad *et al.* 2013; Ducrozet & Gouin 2017; Zheng *et al.* 2020; Zhang & Benoit 2021) have attested heavier tails than expected by Longuet-Higgins (1952). Nonlinearities and abrupt depth change lead waves out of equilibrium, deviating from Gaussian statistics. For a step, these bathymetry effects have been described by nonlinear evolution of interacting free modes with a truncation of the Korteweg–De Vries equation (Majda, Moore & Qi 2019; Moore *et al.* 2020) and as travelling wave packets subject to second-order effects in steepness (Li *et al.* 2021*a*,*c*). However, wave height probability distributions able to describe the laboratory results of Trulsen *et al.* (2020) are still lacking. In fact, Li *et al.* (2021*b*) have obtained a wave crest probability distribution for the step case based on Tayfun (1980), but as it is stated in the section following (36)–(38) of Tayfun (1980), this framework cannot lead to non-Gaussian wave height distributions. The present work seeks a probability distribution for non-homogeneous conditions encountered by waves undergoing rapid depth change. More precisely, we show that regardless of the pre-shoal probability distribution shape, the transformation of the sea surface elevation and spatial energy density through leading second-order effects in steepness will amplify the rogue wave probability. This amplification depends on the dimensionless depth ($k_p h$) and significant steepness (ε).

2. Background and general formulation

Following Massel (2017), we focus on wave and crest heights normalised by the significant wave height $H_{1/3}$, as, respectively,

$$\alpha \equiv \frac{H}{H_{1/3}} = \frac{\mathcal{Z}_c + \mathcal{Z}_t}{H_{1/3}}, \quad \beta \equiv \frac{\mathcal{Z}_c}{H_{1/3}}, \tag{2.1a,b}$$

where $H = \mathcal{Z}_c + \mathcal{Z}_t$ is the crest-to-trough height (hereafter denoted as wave height), $\mathcal{Z}_c$ is the adjacent crest height, and $\mathcal{Z}_t$ is the trough depth. Assuming that we can approximate $H = 2\mathcal{Z}_c$ in narrow-banded seas, the Rayleigh exceedance probability distribution reads (Longuet-Higgins 1952):

$$\mathbb{P}_{\mathcal{R}}(H > \alpha H_{1/3}) \equiv \mathcal{R}_\alpha = \int_\alpha^{+\infty} f_{\alpha_0}\, \mathrm{d}\alpha_0 = \int_\alpha^{+\infty} 4\alpha_0\, \mathrm{e}^{-2\alpha_0^2}\, \mathrm{d}\alpha_0 = \mathrm{e}^{-2\alpha^2}, \tag{2.2}$$

with f_α denoting the probability density function of wave heights. For broader spectra, we define the vertical asymmetry (Kjeldsen 1984; Myrhaug & Kjeldsen 1986) between crest and trough as the ratio between crest and wave height (Linfoot, Stansell & Wolfram 2000). Hence whenever it becomes necessary to convert normalised crests into normalised wave heights in broad-banded seas, they are computed as follows (see § 6.1 of Mendes *et al.* 2021):

$$\mathfrak{S}_0(\alpha) \equiv 2\left\langle \frac{\beta}{\alpha} \right\rangle_r \approx \frac{2\eta_{1/3}}{1+\eta_{1/3}} \left[1 + \frac{2\eta_{1/3}\,\mathrm{Re}\left(\sqrt{\alpha-1}\right)}{7+2\,\mathrm{Re}\left(\sqrt{\alpha-1}\right)} \right], \quad \eta_{1/3} \equiv \left(\frac{\langle \mathcal{Z}_c \rangle_r}{\langle \mathcal{Z}_t \rangle_r} \right)_{H>H_{1/3}}, \tag{2.3}$$

with $\langle\cdot\rangle_r$ denoting a wave record average. Experimental works typically use 20 min records. Remarkably, the vertical asymmetry is related to the skewness μ_3 through the approximation $\eta_{1/3} \approx 1 + \langle\mu_3\rangle_r$ (see (14) and figure 8 of Mendes *et al.* 2021). Moreover, considering the correlation between asymmetry, skewness and significant steepness reported by Guedes Soares, Cherneva & Antao (2004), the asymmetry is weakly dependent on the bandwidth ν due to the bound $\mu_3(1+\nu^2) \lesssim kH_{1/3}$ (Tayfun 2006).

2.1. *Equilibrium wave statistics*

In view of the equivalence between the spectral analysis of spatial and time domains (see Appendix A), we consider the average spatial energy density around x (Dean & Dalrymple 1984), calculated over one spectral zero-crossing wavelength $\bar{\lambda}$ (Massel 2017):

$$\mathcal{E} = \frac{\rho}{2\bar{\lambda}} \int_x^{x+\bar{\lambda}} \left[g\,(\zeta + h(x))^2 + \int_{-h(x)}^{\zeta} (u_1^2 + u_3^2)\, \mathrm{d}z \right] \mathrm{d}x, \tag{2.4}$$

where ρ is the density, g is the gravitational acceleration, h is the water column depth, x is the direction of motion, and z is the vertical axis so that $\boldsymbol{g} = -g\hat{z}$, ζ is the sea surface elevation, and $u_i = \partial\Phi/\partial x_i$ is the ith velocity component derived from the velocity potential. Indeed, the experiments of Trulsen *et al.* (2020) had length of slope 1.6 m while the typical peak wavelength ranged from 1 to 1.8 m, thus validating our calculation above. For an irregular wave field obeying the solution of linear theory (Airy 1845) with

uncorrelated random phases θ_i and amplitudes a_i, one has the surface elevation (Tayfun 1980)

$$\zeta_1(x,t) = \sum_i a_i \cos(k_i x - \omega_i t + \theta_i), \tag{2.5}$$

where the ith components have wavenumber k_i and frequency ω_i. Assuming $\zeta/h \ll 1$ and $\langle\zeta\rangle \approx 0$ for the second integral interval in (2.4) (Dean & Dalrymple 1984), the energy reads

$$\mathcal{E}_{AIRY} = \tfrac{1}{8}\rho g H^2 = \tfrac{1}{2}\rho g a^2, \quad \therefore \quad \mathscr{E}_{AIRY} = \frac{\mathcal{E}_{AIRY}}{\rho g} = \tfrac{1}{2}\sum_i a_i^2, \tag{2.6}$$

where a is the wave train amplitude. Then, using the spatial counterpart of the Khintchine (1934) theorem, which relates the spectral density of a spatial series to its autocorrelation in homogeneous processes, one concludes (see Appendix A) that

$$R_x(\xi = 0) := \mathbb{E}[\zeta^2] = \langle\zeta^2\rangle_x = \int_0^{+\infty} S(k)\,\mathrm{d}k \equiv m_0 = \mathscr{E}_{AIRY}, \tag{2.7}$$

with $S(k)$ denoting the unidirectional ocean energy spectrum based on the wavenumber, which is equivalent to computing the autocorrelation in time and reformulate it in terms of the spectrum $S(\omega)$ for stationarity in time when the system is both homogeneous and stationary (Massel 2017). This water wave solution features a Rayleigh distribution of wave heights in the form $\mathbb{P}(H > H_0) = \mathrm{e}^{-H_0^2/8m_0}$ in an irregular wave field with narrow-banded spectrum (Longuet-Higgins 1952). In the next section we will challenge the assumption of homogeneity implied by the use of the Khintchine (1934) theorem, paving the way for the analysis of non-equilibrium statistics.

3. Non-equilibrium wave statistics

Despite the usefulness of the Airy (1845) formulation for the spectral analysis of water waves, the evolution of the ocean surface is not stationary, spatially homogeneous or ergodic (Cherneva & Guedes Soares 2008; Goda 2010). Therefore, higher-order (unsteady) corrections to the Khintchine (1934) theorem should be considered. During the shoaling, the autocorrelation function is computed from (Here, the surface elevation $\zeta(x,t)$ has been denoted as $\zeta(x)$ to ease the notation.)

$$R_x(\xi, x) = \mathbb{E}[\zeta(x)\,\zeta(x+\xi)] = \int_{-\infty}^{+\infty} \zeta(x)\,\zeta(x+\xi)\,f_{\Gamma(x)}(\zeta)\,\mathrm{d}\zeta, \tag{3.1}$$

where $f_{\Gamma(x)}(\zeta)$ is the probability density of the surface elevation $\zeta(x,t)$ at a fixed point x, and is expected to depend on a correction $\Gamma(x)$ due to the effect of bathymetry. In the spirit of Longuet-Higgins (1980) and Das & Nason (2016), the correction is defined by comparing how the ensemble and spatial energy averages change at and past the shoal, as

$$\Gamma(x) := \frac{\mathbb{E}[\zeta^2(x,t)]}{\mathscr{E}} = \frac{\mathbb{E}[\zeta^2(x,t)](x)}{\mathscr{E}(x)}, \tag{3.2}$$

which means that in a non-homogeneous setting, the surface elevation depends on (x,t) but both ensemble and energy averages depend only on space. Clearly, due to (2.7), $\Gamma \to 1$ both prior to and several wavelengths after the shoal. Without the exact shape of the random phase distribution as in (A7), it is impossible to find the ensemble average

$\mathbb{E}[\zeta^2]$ because the probability density $f_\Gamma(\zeta)$ is unknown: the goal of the present work is to find its wave height counterpart. Since the targeted experiments are stationary in time but non-homogeneous in space, we have that $\mathbb{E}_{x=x_i}[\zeta^2] = \langle\zeta^2\rangle_{t,x=x_i}$, i.e. that the time average equals the ensemble average at any point $x_i \in \mathbb{R}$ of the spatial evolution. Because the evolution of a generalised spatiotemporal autocorrelation can be described as evolutionary spectrum $S(\omega, x)$, like those computed for the targeted experiments (Trulsen *et al.* 2020) whose statistics were generated considering the time series at different locations (Lawrence, Trulsen & Gramstad 2021), we may reduce (3.2) to the spatial evolution of the autocorrelation in time:

$$\Gamma(x) = \frac{R_t(\tau = 0, x)}{\mathscr{E}(x)} = \frac{\mathbb{E}[\zeta(x,t)\,\zeta(x,t+0)]}{\mathscr{E}(x)} \equiv \frac{\langle\zeta(x,t)\,\zeta(x,t+0)\rangle_t}{\mathscr{E}(x)}. \tag{3.3}$$

Note that the spatial and temporal averages are functions not of time but of horizontal displacements, much like the ensemble average. Indeed, for homogeneous processes, it is customary to fix a free parameter A such that the area under the spectral curve is equal to the mean power (Massel 2017), e.g. $R_x(\xi = 0) = \int_0^\infty S(k)\,\mathrm{d}k$ for a one-sided spectrum. Instead, we choose A such that the area under the spectral curve matches the spatial energy density ($\mathscr{E}$) during homogeneous stages, and it reduces to the autocorrelation in the Gaussian case, i.e. in the strictly homogeneous case prior to the shoal. For non-homogeneous processes, this is not the case, and the methods for finding a spectrum produce anomalies and undesirable features (Loynes 1968; Cohen 1989; Flandrin 1989; Adak 1995; Bruscato & Toloi 2004). This implies that there is no canonical or unique way to define a non-homogeneous Khintchine theorem (Flandrin 1989) such that the ratio $\mathbb{E}[\zeta^2]/\mathscr{E}$ computes the deviation from homogeneity. On the other hand, there are ergodic theorems for non-stationary (or non-homogeneous) processes that we will not discuss in detail; see, for instance, Nagabhushanam & Bhagavan (1969) and Salehi (1973), and references therein. In practice, we may speak of an ergodic approximation for non-homogeneous process in which the cumulative integral of the ensemble average in a given interval in x is well approximated by the spatial average over the same interval, so that we could have had $\Gamma(x) = R_x(\xi = 0, x)/\mathscr{E}(x)$ as long as the spatial series is sufficiently long, and thus it converges to the ensemble average. For simplicity, we henceforth use the notation $\langle\zeta^2\rangle$ for the temporal average, while in the appendices we specify whether we speak of temporal or spatial averaging.

Let us now focus on how the wave statistics will adapt to a non-homogeneous correction parameter Γ in the ocean. To first order, the probability density of wave heights must fulfil the narrow-band identity

$$\int_0^{+\infty} f(H)\,H^2\,\mathrm{d}H = 8\langle\zeta^2\rangle. \tag{3.4}$$

Due to the difficulty of converting surface elevation distributions into crest and height distributions in broad-banded seas (Janssen 2014), (3.4) replaces the typical envelope approach to find the wave height distribution directly. Therefore, neglecting skewness μ_3 and kurtosis μ_4, the change in the ratio $\langle\zeta^2\rangle/m_0 \to \Gamma \times (\langle\zeta^2\rangle/m_0)$ applied to (2.2) relates the $2\alpha^2$ to $\langle\zeta^2\rangle/m_0$, resulting in the narrow-banded correction

$$\mathcal{R}_{\alpha,\Gamma}(H > \alpha H_{1/3}) = \int_\alpha^{+\infty} \frac{4\alpha_0}{\Gamma}\,\mathrm{e}^{-2\alpha_0^2/\Gamma}\,\mathrm{d}\alpha_0 = \mathrm{e}^{-2\alpha^2/\Gamma}; \tag{3.5}$$

that is, the initial wave train Gaussian statistics will be affected by bathymetry, and its exceedance probability $\mathcal{R}_\alpha$ will be transformed into $\mathcal{R}_{\alpha,\Gamma}$ by the shoaling process.

Following the same energetics argument as in § 2.1, let us generalise the velocity potential (Dingemans 1997) and surface elevation in (2.5) to an irregular wave field subject to second-order effects in steepness, with uncorrelated random amplitudes and phases (a brief discussion is provided in Appendix A) given by

$$\left.\begin{aligned}\Phi(x,z,t) &= \sum_i \sum_m \frac{\Omega_{m,i}(k_i h)}{m k_i}\cosh(m\varphi)\sin(m\phi),\\ \zeta(x,t) &= \sum_i \sum_m \tilde{\Omega}_{m,i}(k_i h)\cos(m\phi),\end{aligned}\right\} \tag{3.6}$$

with the auxiliary variables $\varphi = k_i(z+h)$ and $\phi = k_i(x - c_{m,i}t + \theta_i)$, where $c_{m,i} = c_m(k_i)$ is the phase velocity of the ith spectral component of mth order in steepness. To allow an analytical treatment, the above expression for surface elevation contains no directional effects or wave–wave interaction, and is restricted to the super-harmonic term of the second-order correction. This approximation is supported by Dingemans (1997) and Forristall (2000). In fact, sub-harmonics are at least one order of magnitude smaller than the super-harmonic (see figure 7 of Li *et al.* 2021*c*), and given that the super-harmonic contributes to only a 2–3 % change in the energy correction due to shoaling, one should expect the sub-harmonic term to not be fundamental to our analysis. Due to this approximation, however, the treatment is not equivalent to Stokes waves, whose propagation in deep water having a narrow-banded spectrum leads to the modulational instability (Dysthe *et al.* 2008; Zakharov & Ostrovsky 2009; Onorato *et al.* 2013).

Under the framework above, we subtract the fixed depth $h_0^2/2$ term from the energy and can prove for a depth variation $\partial h(x)/\partial x \ll 1$ (see Appendix B) that

$$\langle \zeta^2 \rangle = \frac{1}{2}\sum_i \sum_m \tilde{\Omega}_{m,i}^2, \quad \mathscr{E} = \frac{1}{4}\sum_i \sum_m \left[\tilde{\Omega}_{m,i}^2 + \Omega_{m,i}^2 \frac{\sinh(2mkh)}{2mgk}\right]. \tag{3.7a,b}$$

In the limit $i \to \infty$, we can treat the leading-order coefficients $(\Omega_m, \tilde{\Omega}_m)$ as being decomposed into a series of even powers of steepness coupled to factored out trigonometric functions $(\chi_m, \tilde{\chi}_m)$ (see Appendix B), leading to

$$\left.\begin{aligned}\mathscr{E} &= \frac{a^2}{4}\left[1 + \left(\frac{\pi\varepsilon}{4}\right)^2 \chi_1 + \cdots\right] + \frac{a^2}{4}\left[1 + \left(\frac{\pi\varepsilon}{4}\right)^2 \tilde{\chi}_1 + \cdots\right],\\ \langle \zeta^2 \rangle &= \frac{a^2}{2}\left[1 + \left(\frac{\pi\varepsilon}{4}\right)^2 \tilde{\chi}_1 + \left(\frac{\pi\varepsilon}{4}\right)^4 \tilde{\chi}_2 + \cdots\right].\end{aligned}\right\} \tag{3.8}$$

Hence, due to the expressions in (3.3) we get

$$\Gamma \approx \frac{\langle \zeta^2 \rangle}{\mathscr{E}} = \frac{1 + \sum_p \left(\frac{\pi\varepsilon}{4}\right)^{2p} \tilde{\chi}_p}{1 + \frac{1}{2}\sum_p \left(\frac{\pi\varepsilon}{4}\right)^{2p} (\tilde{\chi}_p + \chi_p)}. \tag{3.9}$$

This expression demonstrates that the effect of energetics is reduced to the coefficients of (3.8). We assume that waves before the shoal propagate on a flat bottom and follow the Gaussian distribution associated with the linear wave theory. Afterwards, due to the bathymetry change, second-order corrections become relevant since a

much larger steepness is to be taken into account (see Eagleson 1956). Consequently, out-of-equilibrium dynamics will deform an initially Gaussian distribution due to higher-order effects in steepness. In order to apply the same correction to an arbitrary initial distribution, Appendix C shows that modelling any bathymetry change by a transition from first- to second-order terms is very effective. The Γ correction depends only on ε and kh. Additionally, it is independent of slope of the shoaling, provided that the latter is sufficiently steep (Zheng *et al.* 2020). Thus it is applicable to the Trulsen *et al.* (2020) experiments that featured a slope of 1/3.8. Indeed, results by Gramstad *et al.* (2013) suggest that the rogue wave probability is an order of magnitude more sensitive to a relative change in dimensionless depth $k_p h$ than in the slope of the shoal. Recently, Fu *et al.* (2021) has also demonstrated that for steep-shoaling slopes, the probability of rogue waves remains the same.

3.1. *Second-order statistics*

Under the validity of the above assumptions, the spatial energy density for a second-order perturbation in the narrow-banded case reads (see (B9))

$$\mathcal{E} = \frac{1}{2}\rho g a^2 \left[1 + \left(\frac{\pi\varepsilon}{4}\right)^2 \left(\frac{\tilde{\chi}_1 + \chi_1}{2}\right)\right], \quad ka = \pi\varepsilon \times \mathfrak{S}_0, \tag{3.10a,b}$$

with coefficients reading (see figure 1*a*)

$$\tilde{\chi}_1 = \left[\frac{\cosh kh\,[2 + \cosh(2kh)]}{\sinh^3 kh}\right]^2, \quad \chi_1 = \frac{9\cosh(2kh)}{\sinh^6 kh}. \tag{3.11a,b}$$

This model is valid provided that the Ursell number is $Ur = H\lambda^2/h^3 = \varepsilon(2\pi/kh)^3 \leqslant 8\pi^2/3$ (Lé Méhaute 1976; Dean & Dalrymple 1984). Hence, for small amplitudes ($\zeta \ll h$),

$$\mathscr{E} = \frac{1}{2}\sum_i a_i^2 + \frac{\pi^2}{16}(\tilde{\chi}_1 + \chi_1)\sum_i \frac{a_i^4}{\lambda_i^2} \equiv m_0, \tag{3.12}$$

whereas the surface total variance reads

$$\langle\zeta^2\rangle = \frac{1}{2}\sum_i a_i^2 + \frac{\tilde{\chi}_1\pi^2}{8}\sum_i \frac{a_i^4}{\lambda_i^2}. \tag{3.13}$$

In order to consider the whole ensemble of waves, we employ the wavenumber at the peak of the spectrum, k_p, in the dimensionless depth $k_p h$, and the zero-crossing wavelength $\bar{\lambda}$ in the significant steepness $\varepsilon = H_{1/3}/\bar{\lambda}$ (Massel 2017). Thus, in the limit of a large number of wave components, the previous expressions read

$$\frac{2\langle\zeta^2\rangle}{a^2} = 1 + \left(\frac{\pi\varepsilon}{4}\right)^2 \tilde{\chi}_1, \quad \frac{2\mathscr{E}}{a^2} = 1 + \left(\frac{\pi\varepsilon}{4}\right)^2 \frac{(\tilde{\chi}_1 + \chi_1)}{2}. \tag{3.14a,b}$$

The narrow-banded correction for a group of waves over a changing bathymetry is

$$\Gamma = \frac{\langle\zeta^2\rangle}{\mathscr{E}} = \frac{32 + 2\tilde{\chi}_1\pi^2\varepsilon^2}{32 + (\tilde{\chi}_1 + \chi_1)\pi^2\varepsilon^2} \approx 1 + \left(\frac{\pi\varepsilon}{4}\right)^2 \left(\frac{\tilde{\chi}_1 - \chi_1}{2}\right). \tag{3.15}$$

Γ exceeds 1 for all depths, with a maximum of up to 1.13 in intermediate depths ($k_p h \sim$ 0.5–1) and an asymptotic behaviour for deep water (see figure 1*b*). This shape defines three

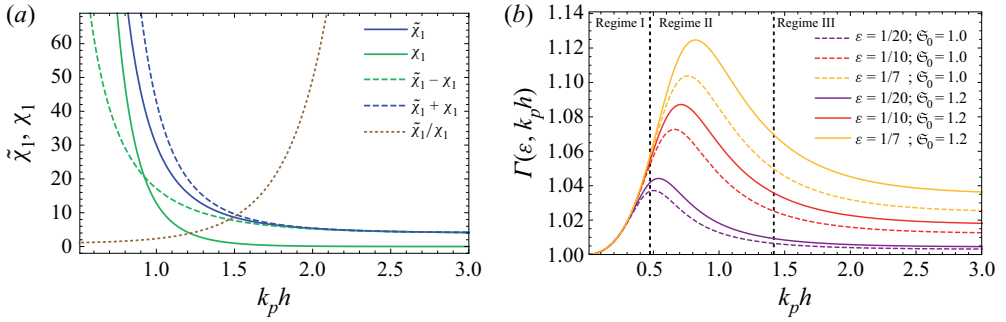

Figure 1. (*a*) Trigonometric coefficients (χ_m, $\tilde{\chi}_m$) of the second-order model. (*b*) Correction parameter Γ as a function of steepness $\varepsilon = H_{1/3}/\bar{\lambda}$ and dimensionless depth $k_p h$ in both narrow-banded ($\mathfrak{S}_0 = 1.0$) and broad-banded ($\mathfrak{S}_0 = 1.2$) seas.

regimes, as marked in figure 1(*b*). In shallow water (Regime I), a shoal reducing the depth will reduce Γ, hence the exceedance probability. Conversely, beyond the maximum of Γ (Regime II), the shoal will increase Γ and the exceedance probability. Finally, as long as the shoal stays within Regime III, the depth variation will translate into a negligible change in Γ, hence will have no consequence for the exceedance probability. Such absence in amplification is similar to the second-order height distribution in Tayfun (1980) in deep water (see § 3.5). This behaviour will allow us to simplify investigations of shoals starting in deep water ($k_p h \gtrsim 2$), well within Regime III. We can without loss of generality start the analysis of the wave statistics evolution at the point when it enters Regime II.

In order to generalise the derivation of (3.15) to broad-band seas, we use the definition of asymmetry from (2.3). Consequently, the steepness in (3.10*a*,*b*)–(3.15) will be corrected by the vertical asymmetry $\mathfrak{S}_0$, which in turn modifies the correction parameter:

$$\Gamma_{\mathfrak{S}_0}(\varepsilon, k_p h) = \frac{32 + 2\tilde{\chi}_1 \mathfrak{S}_0^2 \pi^2 \varepsilon^2}{32 + (\tilde{\chi}_1 + \chi_1)\mathfrak{S}_0^2 \pi^2 \varepsilon^2}. \tag{3.16}$$

The vertical asymmetry will increase the correction $\Gamma_{\mathfrak{S}_0}$ as compared to the narrow-band case by a few percent, as follows (see figure 1*b*):

$$\frac{\Gamma_{\mathfrak{S}_0}(\varepsilon, k_p h)}{\Gamma(\varepsilon, k_p h)} \approx 1 + \frac{1}{2}(\tilde{\chi}_1 - \chi_1)(\mathfrak{S}_0^2 - 1)\left(\frac{\pi\varepsilon}{4}\right)^2 + O(\varepsilon^4). \tag{3.17}$$

On the other hand, the parameter Γ must be corrected for wave breaking, leading to slightly smaller peaks (see figure 2*a*). We include a depth-dependent breaking limit of regular waves (Miche 1944) by setting $\varepsilon \leqslant (\varepsilon_0/7)\tanh k_p h$ with $0 \leqslant \varepsilon_0 \leqslant 1$:

$$\Gamma_{\mathfrak{S}_0,0} \approx \frac{1600 + 2\pi^2 \mathfrak{S}_0^2 \varepsilon_0^2 \tilde{\chi}_1 \tanh^2 k_p h}{1600 + \pi^2 \mathfrak{S}_0^2 \varepsilon_0^2 (\tilde{\chi}_1 + \chi_1)\tanh^2 k_p h}, \tag{3.18}$$

where even if the ratio ε_0 is constant, the actual (breaking-limited) steepness ε will drop considerably throughout the transition from deep to shallow waters (see figure 2*a*). The vertical asymmetry $\mathfrak{S}_0$ increases the value of Γ significantly (figure 2*b*), but less than the decrease in Γ due to wave breaking. Although (3.17) typically increases the shoal correction by a few percent, it also shows that the correction has an upper bound $\Gamma \leqslant 1.20$ when $\varepsilon_0 = 1$ and $k_p h = 0.5$, and maximum possible asymmetry $\mathfrak{S}_0 = 2$ (skewed sea with $\eta_{1/3} \approx 2.1$). Therefore, a decrease in the depth $k_p h$ as in the experiments of Trulsen *et al.*

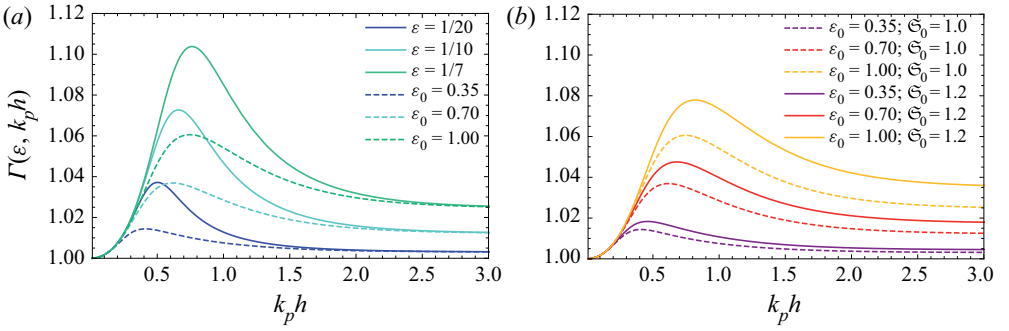

Figure 2. Γ correction parameter with the same initial significant steepness in deep water (*a*) with (dashed) or without (solid) wave breaking in narrow-banded seas, and (*b*) accounting for wave breaking in narrow-banded (dashed) and broad-banded (solid) seas.

(2020) will increase the significant steepness as well as Γ, hence $\mathcal{R}_{\alpha,\Gamma}$ given in (3.5), i.e. the probability of rogue waves as compared to the pre-shoal, homogeneous Rayleigh distribution towards Regime II.

3.2. *The normalised height diagram*

Since a bandwidth correction to the standard measure $H_{1/3} = 4\sigma$ will affect the Rayleigh distribution (Longuet-Higgins 1980), such a relation provides a valuable test for the Rayleigh distribution (Goda 1983). Hence the distribution of wave heights contains information on the ratio $H_{1/3}/\sigma$, as follows:

$$\exp\left(-\frac{H^2}{8m_0}\right) = \exp\left(-\frac{H^2}{8H_{1/3}^2}\left(\frac{H_{1/3}}{\sqrt{m_0}}\right)^2\right) \equiv \exp\left(-\frac{\alpha^2}{8}\left(\frac{H_{1/3}}{\sqrt{m_0}}\right)^2\right), \tag{3.19}$$

which shows that at fixed energy (fixed $m_0 = \sigma^2$), the change in the ratio $H_{1/3}/\sigma$ is balanced by the normalisation $\alpha = H/H_{1/3}$, therefore the overall exponent stays invariant, thus the wave statistics. However, if and only if m_0 increases in comparison to Airy's solution, we expect the coefficient $H_{1/3}^2/m_0$ attached to α^2 to be smaller. In fact, this can be seen by the ratio of the energies at first order (2.6) and second order (3.10*a*,*b*). To investigate the effect of broad-band seas on $H_{1/3}/\sigma$ by the direct measurement of the vertical asymmetry as in (2.3), we combine (3.5) and (3.19), and find (see figure 3*a*)

$$H_{1/3} = \frac{4}{\mathfrak{S}_0}\sqrt{\frac{m_0}{\Gamma_{\mathfrak{S}_0}}}. \tag{3.20}$$

Consequently, the ratios $H_{1/3}/\sqrt{m_0}$ obtained from our model agree with the asymptotic values of 4 (narrow-banded in deep water, solid lines) and 3.8 (broad-banded in deep water, dashed line), as reported by Goda (1983). Asymmetry contributes to this expression via two different processes. On one hand, the $1/\mathfrak{S}_0$ factor corresponds to its direct influence on the significant wave height. This factor does not depend on the occurrence of a shoal, although the asymmetry depends ultimately on the depth. Increasing the bandwidth and therefore $\mathfrak{S}_0$ will also lower $H_{1/3}/\sigma$ (see (3.20)), as demonstrated by Vandever *et al.* (2008). On the other hand, the asymmetry influences the probability amplification by the shoal, via its impact on $\Gamma_{\mathfrak{S}_0}$. Except in very shallow water (Regime I), both $\mathfrak{S}_0$ and $\Gamma_{\mathfrak{S}_0}$ decrease monotonically as a function of $k_p h$, as we model the pre-shoal zone

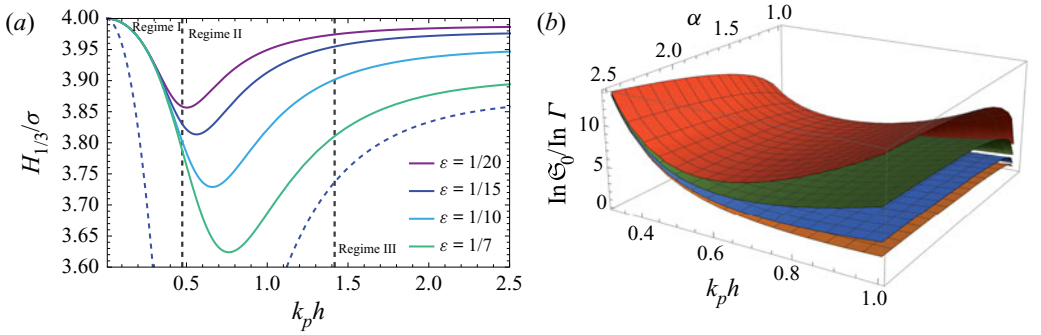

Figure 3. (*a*) H–σ diagram for narrow-banded $\mathfrak{S}_0 = \sqrt{\Gamma}$ (solid) and otherwise with $\mathfrak{S}_0 \sim \Gamma^2$ (dashed) for the specific case of $\varepsilon = 1/15$ for comparison. (*b*) Ratio $\kappa = \ln \mathfrak{S}_0 / \ln \Gamma$ with steepness: 1/7 (orange), 1/10 (blue), 1/15 (green) and 1/20 (red).

as a homogeneous Airy solution concurrently leading to $\mathfrak{S}_0 \to 1$ and $\Gamma_{\mathfrak{S}_0} \to 1$. We can therefore define a parameterisation mapping the latter to the former, in the form $\mathfrak{S}_0 = \Gamma_{\mathfrak{S}_0}^{\kappa}$ (figure 3*b*), or, equivalently, its linear version $\mathfrak{S}_0 = 1 + \kappa(\Gamma_{\mathfrak{S}_0} - 1)$. Note that this parameterisation aims to describe the simultaneous evolution of Γ and the asymmetry when the depth evolves, while (3.17) describes only the direct impact of the asymmetry on Γ. Since Regime II is the one where we seek the evolution of the exceedance probability, the κ parameterisation appears suitable for our work. Furthermore, its use avoids the numerical issues that would arise if handling $\mathfrak{S}_0$ and Γ as independent.

3.3. *Evolution of a narrow-banded arbitrary probability distribution*

So far, we have studied a pre-shoal Rayleigh distribution of the surface elevation. Following (3.5), the Γ correction due to a rapid bathymetry change reads

$$\mathcal{R}_{\alpha,\Gamma} = \mathrm{e}^{-2\alpha^2/\Gamma} = (\mathcal{R}_\alpha)^{1/\Gamma} \quad \therefore \quad \frac{\ln \mathcal{R}_\alpha}{\Gamma \ln \mathcal{R}_{\alpha,\Gamma}} = 1, \tag{3.21}$$

$$\frac{\mathcal{R}_{\alpha,\Gamma}}{\mathcal{R}_\alpha} = (\mathcal{R}_\alpha)^{(1/\Gamma - 1)} = \exp\left(2\alpha^2\left(1 - \frac{1}{\Gamma}\right)\right). \tag{3.22}$$

The same correction therefore applies to any initial surface elevation distribution $\mathbb{P}$, as detailed in Appendix C. For a narrow-banded sea,

$$\mathbb{P}_{\alpha,\Gamma} \approx (\mathbb{P}_\alpha)^{1/\Gamma} \quad \therefore \quad \frac{\mathbb{P}_{\alpha,\Gamma}}{\mathbb{P}_\alpha} \approx \exp\left(2\alpha^2\left(1 - \frac{1}{\Gamma}\right)\right), \tag{3.23}$$

where $\mathbb{P}_\alpha$ denotes the exceedance probability at equilibrium prior to the shoal, and $\mathbb{P}_{\alpha,\Gamma}$ is the distribution within the non-equilibrium zone. Hence the highest possible realistic values of $\Gamma \sim 1.08$ (see figure 1) lead to a two-fold increase of rogue wave probability.

3.4. *Evolution of a broad-banded arbitrary probability distribution*

In the case of a broad-banded sea, the connection between crest and height statistics responsible for (3.20) can be reinterpreted as a simple change of variables $\Gamma \to \mathfrak{S}_0^2 \Gamma_{\mathfrak{S}_0}$

in (3.5), so that (3.23) becomes

$$\mathbb{P}_{\alpha,\Gamma_{\mathfrak{S}_0}} \approx (\mathbb{P}_\alpha)^{1/\mathfrak{S}_0^2\Gamma_{\mathfrak{S}_0}} \quad \therefore \quad \frac{\mathbb{P}_{\alpha,\Gamma_{\mathfrak{S}_0}}}{\mathbb{P}_\alpha} \approx \exp\left(2\alpha^2\left(1-\frac{1}{\mathfrak{S}_0^2\Gamma_{\mathfrak{S}_0}}\right)\right). \tag{3.24}$$

To ensure the numerical stability of the distribution along the propagation, we use the κ parameterisation introduced in § 3.2. For practical purposes, we estimate it as

$$\kappa_0 = \frac{\ln\left[\max \mathfrak{S}_0\right]}{\ln\left[\max \Gamma\left(\langle\varepsilon\rangle, k_p h, \mathfrak{S}_0\right)\right]} \approx \frac{\ln \mathfrak{S}_0}{\ln \Gamma\left(\langle\varepsilon\rangle, k_p h, \mathfrak{S}_0\right)}, \tag{3.25}$$

where the maximum of Γ is taken over the propagation on the whole shoal, $\langle\varepsilon\rangle$ being the average of the pre- and post-shoal steepness. It can be measured at both stages of the wave propagation, or, alternatively, obtained from forecast or hindcast, from the zero-crossing period and significant wave height. Note that uncertainties in asymmetry impact marginally the value of κ_0, as respective errors in the numerator and in Γ tend to partially compensate for each other due to (3.17). Consequently, the effect of the shoal on the exceedance probability evolves during the propagation along x as

$$\frac{\ln \mathbb{P}_\alpha}{\ln \mathbb{P}_{\alpha,\Gamma}} = \mathfrak{S}_0^2 \times \Gamma = \left[\Gamma\left(\langle\varepsilon\rangle, k_p h, \mathfrak{S}_0\right)\right]^{2\kappa_0} \times \Gamma\left(\varepsilon(x), k_p h(x), \mathfrak{S}_0\right). \tag{3.26}$$

When the evolution spreads into Regimes I and III, the use of κ_0 is necessary to avoid divergence, though a continuous κ restricted to Regime II is applicable. Note that under adequate conditions, a more compact form can be derived, as detailed in Appendix D.

3.5. *Comparison with standard second-order models*

In this subsection, we delineate similarities and differences between our model of second-order wave height probability and the typical treatment arising from Tayfun (1980). Following the second-order water surface, one finds (Tung & Huang 1985)

$$\zeta(\phi=0) := \mathcal{Z}_c = \left[a\cos\phi + \frac{ka^2}{2}\cos(2\phi)\right]_{\phi=0} = a + \frac{ka^2}{2}, \tag{3.27}$$

which, normalised by the variance, reduces (with nomenclature $\sigma\tilde{X} := X$) to

$$\tilde{\mathcal{Z}}_c = \tilde{a} + \tilde{a}^2 \times \frac{k\sigma}{2} \quad \therefore \quad \tilde{a} = \frac{\sqrt{1+2\tilde{\mathcal{Z}}_c\sigma k}-1}{\sigma k}. \tag{3.28}$$

Applying the finite-depth coefficients in (2.382*a*) of Dingemans (1997), one finds

$$\tilde{\mathcal{Z}}_c = \tilde{a} + \tilde{a}^2 \times \frac{k\sigma}{2} \times \mathcal{F}, \quad \mathcal{F} = \mathcal{F}(kh) = \frac{3-\tanh^2 kh}{2\tanh^3 kh}, \tag{3.29a,b}$$

leading to the mathematical structure (see Mendes *et al.* (2021) for the $\mathcal{F}=1$ case)

$$\mathbb{P}(H > \alpha H_{1/3}) = \exp\left\{-\frac{8}{k^2 H_{1/3}^2 \mathcal{F}^2}\left[\sqrt{1+\alpha k H_{1/3}\mathcal{F}}-1\right]^2\right\}. \tag{3.30}$$

Note, however, that this distribution was not derived in the narrow-band model of Tayfun (1980); it is rather an adaptation to extract the mathematical structure of a probability

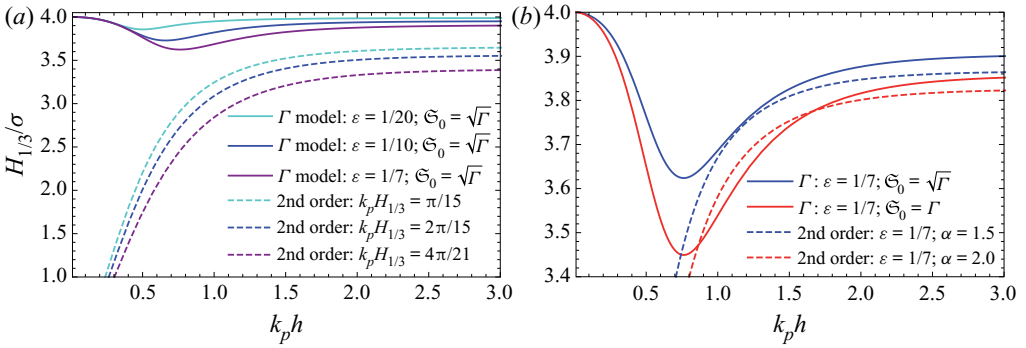

Figure 4. (*a*) Γ model (solid) as compared to the finite-depth adjusted second-order structure (dashed), and (*b*) with corrected steepness.

growing boundlessly with increasing steepness. Although Tayfun (2006) puts limitations on the steepness as $\mu_3 \lesssim kH_{1/3}/(1+\nu^2)$, North Sea data (Stansell 2004; Mendes *et al.* 2021) shows that the skewness can grow higher. Therefore, the suggested adaptation to wave heights is useful since now ε can reach its breaking limit (Miche 1944). In figure 4(*a*), we compare our Γ model of (3.24) with that of (3.30) through the H–σ diagram:

$$\frac{H_{1/3}}{\sqrt{m_0}} = \frac{8}{\alpha k H_{1/3}\mathcal{F}}\left[\sqrt{1+\alpha k H_{1/3}\mathcal{F}} - 1\right]. \tag{3.31}$$

The finite-depth adapted height model yields 10–20 % lower ratios in deep water, and drops towards zero in shallow water, in contradiction with observations (Goda 1983). Nonetheless, our model can be consistent with the structure of (3.30) in both deep and transitional waters ($k_ph \geqslant 0.8$) for moderate values of α and within the narrow-band validity of Tayfun (1980), provided that (3.30) is corrected to the steepness $k_pH_{1/3} \to \varepsilon_s$, where $\varepsilon_s := \langle\varepsilon_i\rangle_r = \langle H_{1/3}/\lambda_i\rangle_r$; see figure 4(*b*). Indeed, we can use $\langle\lambda_i\rangle_r \approx 1.5\bar{\lambda}$ (Mendes *et al.* 2021), which implies $\varepsilon = H_{1/3}/\bar{\lambda} \approx 1.5\varepsilon_s \approx 3kH_{1/3}/4\pi$. For transitional and especially shallower regions reaching the limit of the second-order approximation, the above adapted model would not reproduce the same probability amplification as our model, nor the original one (Tayfun 1980). Hence our model departs from Tayfun (1980) in finite depth and recovers it in deep water.

4. Comparison with Trulsen experiments

Raustøl (2014) provides experiments of wave propagation over a shoal, later summarised in Trulsen *et al.* (2020). These experiments were carried out in a 24.6 m long and 0.5 m wide wave tank. Surface elevation measurements were made with ultrasound probes, and velocity measurements were made with an acoustic doppler velocimeter, with an array of 16 probes that was moved to four different locations such that the resolution before the shoal was 0.3 m and the resolution above the shoal was 0.1 m. The wavemaker generated a JONSWAP spectrum with peak parameter $\gamma = 3.3$, with typical peak periods $T_p \sim 1$ s. The probability distribution of rogue waves evolving with the distance from the wavemaker was recorded, offering a benchmark for our non-homogeneous correction to the wave height probability distribution. Since our model is expressed in terms of dimensionless depth and significant steepness, we have extracted the raw data from figures 5.4 and 5.5 of Raustøl (2014), in accordance with the inversion $k_ph \approx (k_pa_c/Ur)^{1/3}$ of Trulsen *et al.* (2020). In order to facilitate the processing, we have smoothed the

experimental data by fitting analytic functions on the data points, as described in detail in Appendix E. The experiments feature a shoal starting at $x = 0$, rising up to 42 cm at $x = 1.6$ m, followed by a plateau until $x = 3.2$ m and a decay to zero until $x = 4.8$ m. The initial depth ranges between 50 and 60 cm depending on the runs, as detailed in table 1 of Trulsen *et al.* (2020) and table 5.2 of Raustøl (2014).

4.1. *Results*

Based on the κ_0 parameterisation described in the previous section, we compute the evolution of the rogue wave probability as a function of distance for each run, assuming a pre-shoal homogeneous Rayleigh distribution (figure 5). The values of κ_0 calculated according to (3.25) amount to (5.9, 4.9, 4.3, 3.6, 2.9, 2.6, 2.3, 2.4, 2.3, 2.2) for the runs 1–2, 4–9 and 11–12, respectively. Our model that takes into account the evolution of the wave asymmetry $\mathfrak{S}_0$ over the shoal (cyan curves) due to the skewness of the surface elevation distribution (2.3) reproduces well the experimental data, over the whole shoaling episode and for all runs. Disregarding the evolution of skewness reported in Trulsen *et al.* (2020) while keeping a vertical fixed asymmetry $\mathfrak{S}_0 = 1.2$ (blue curves in figure 5) degrades the agreement only marginally, although the probability rises slightly earlier, decays slightly later, and the asymmetry between the up- and down-shoaling phases is reduced. Furthermore, we point out the remarkable difference of amplification between vertically asymmetrical (solid blue, cyan) and symmetrical seas (dashed red). This happens because (3.21) leads to a maximal amplification between 75 % and 100 % for $\Gamma \approx 1.08$–1.10. When we include the typical vertical asymmetry $\mathfrak{S}_0^2 \sim 1.5$, the pre-shoal probability $\mathbb{P}_\alpha$ is transformed into $\mathbb{P}_\alpha^{2/3} \sim 10\mathbb{P}_\alpha$ within Regime II, seemingly becoming an alternative to Gram–Charlier models (Mori & Yasuda 2002). Finally, adjusting the homogeneous pre-shoal probability to the observed values instead of considering an initial Rayleigh distribution (dotted curve) improves the agreement (runs 6–12, figures 5*e–j*), demonstrating the applicability of our model to arbitrary probability distributions. This agreement over the whole range of experimental conditions reported by Raustøl (2014) is remarkable, as it requires no specific parameter tweaking.

4.2. *Discussion*

In contrast, Tayfun (1980) (see the discussion following (36)–(38) of that paper) claims a Gaussian probability distribution for the second-order wave heights, as also discussed in Tayfun (1990) and Tayfun & Fedele (2007). In fact, these models fall under the broad category of quasi-determinism theories (Boccotti 2000), in which Longuet-Higgins (1980) and Naess (1985) also take part and preclude wave heights from exceeding the Rayleigh distribution, typically being lower than the latter as the bandwidth broadens. Therefore, these formulations in homogeneous conditions would not be able to describe the Raustøl (2014) and Trulsen *et al.* (2020) experiments. Also according to these models, any departure from a Rayleigh distribution of wave heights is due to third-order nonlinearities (Tayfun & Fedele 2007; Alkhalidi & Tayfun 2013). Nevertheless, it is important to remark that most of these theories were devised for deep waters, hence they fall within Regime III of our model. Moreover, following Marthinsen (1992) and Dingemans (1997), one can tentatively elaborate alternative finite-depth second-order mathematical structures as in § 3.5. Comparing with our model, we observe a numerical equivalence in deep water, but not in transitional and shallow waters where the alternative second-order models display a sharp departure from the observations of Goda (1983). Unfortunately, the finite-depth

model of Tayfun & Alkhalidi (2020) is not a distribution of wave heights, hence is not applicable to our discussion.

Our Γ model of the probability evolution over a shoal is based on the second-order correction, which is valid for $Ur \leqslant 8\pi^2/3$ (Dean & Dalrymple 1984). This limit of validity is well beyond the Ursell number $Ur \leqslant 0.22$ of the experiments considered in this work (Raustøl 2014; Trulsen *et al.* 2020). We can therefore expect that the Γ model will still apply to more than 10 times larger waves and/or shallower waters.

The transient drop of $\mathbb{P}_{\alpha,\Gamma}/\mathbb{P}_\alpha$ to almost zero in the rising region of the shoal ($0 \leqslant x \leq 1.6$ m) in runs 1, 2, 4 and 5, as well as its slow decay on the trailing side ($3.2 \leq x \leq 4.8$ m), could be due to higher-order nonlinear effects not captured in our model, including the evolution of the skewness and kurtosis of the surface elevation probability distribution when propagating on the shoal.

Recent developments in Zhang & Benoit (2021) described the exceedance probability of Run 3 of Trulsen *et al.* (2020) throughout the shoaling and de-shoaling stages by means of numerical simulations. However, an analytical expression for the probability distribution was not provided, and cases with low or vanishing skewness and kurtosis like Run 12 were not addressed. Our model provides an explicit expression with no free fitting parameter. It is obtained directly from second-order correction and has been shown to be valid for all runs in Raustøl (2014). Although we were not able to analyse Run 3 (Jorde 2018) due to the lack of wave height probability data, we are confident that our model can reproduce it well, as it does for the very similar Runs 1, 2 and 4.

The modulational instability cannot account for the rise of the rogue wave probability due to shoaling in the considered experiments because they do not feature narrow-banded Stokes waves or lie in the optimal range $k_ph > 1.36$ (Zakharov & Ostrovsky 2009) in the shallower side, except for Runs 11 and 12, which showed no significant amplification. On the other hand, all runs start in the range $k_ph > 1.36$ before the shoal and showed no large deviation from the Gaussian sea, except for Run 12.

Furthermore, our model – and in particular the three regimes discussed in (3.15) and figure 1(*b*) – also allows us to understand the contradictory behaviours highlighted by Trulsen *et al.* (2020) and Zhang & Benoit (2021). While the rogue wave probability is not affected by a shoal in initially deep water (Regime III), it does increase on a shoal in intermediate depth (Regime II). Interestingly, a third regime (Regime I of figure 1*b*) is consistent with observed surf zone statistics (Glukhovskii 1966), i.e. rogue wave likelihood lower than in transitional waters. In addition, Barbariol *et al.* (2015) show an increase of maximum crest up to some cut-off in dimensionless depth, upon which it starts to decrease sharply the higher the ratio $H_{1/3}/h$ becomes, thus providing support for Regime I in our model. However, numerical simulations and experiments with even shallower shoals are necessary for a conclusive assessment. Therefore, we have demonstrated that rogue wave statistics will be enhanced by non-equilibrium dynamics of rapid depth change for a dimensionless depth $0.5 < k_ph < 1.5$ but stops growing when it leaves this range. It is therefore less pronounced past the threshold $k_ph \leqslant 0.3$ until it starts to follow shallow water distributions such as in Glukhovskii (1966). Recently, after the submission of this work, experiments on the shoaling of irregular unidirectional waves have confirmed our prediction that the amplification of wave height statistics in Regime II will vanish in Regime I (Xu *et al.* 2021).

The evolution of the rogue wave probability highlighted by our model could be related to the process proposed by Li *et al.* (2021*c*) and confirmed experimentally in Li *et al.* (2021*a*), in which the generation of additional wave packets that interact with the original pre-shoal wave packet propagating over a step leads to a local peak some distance into the

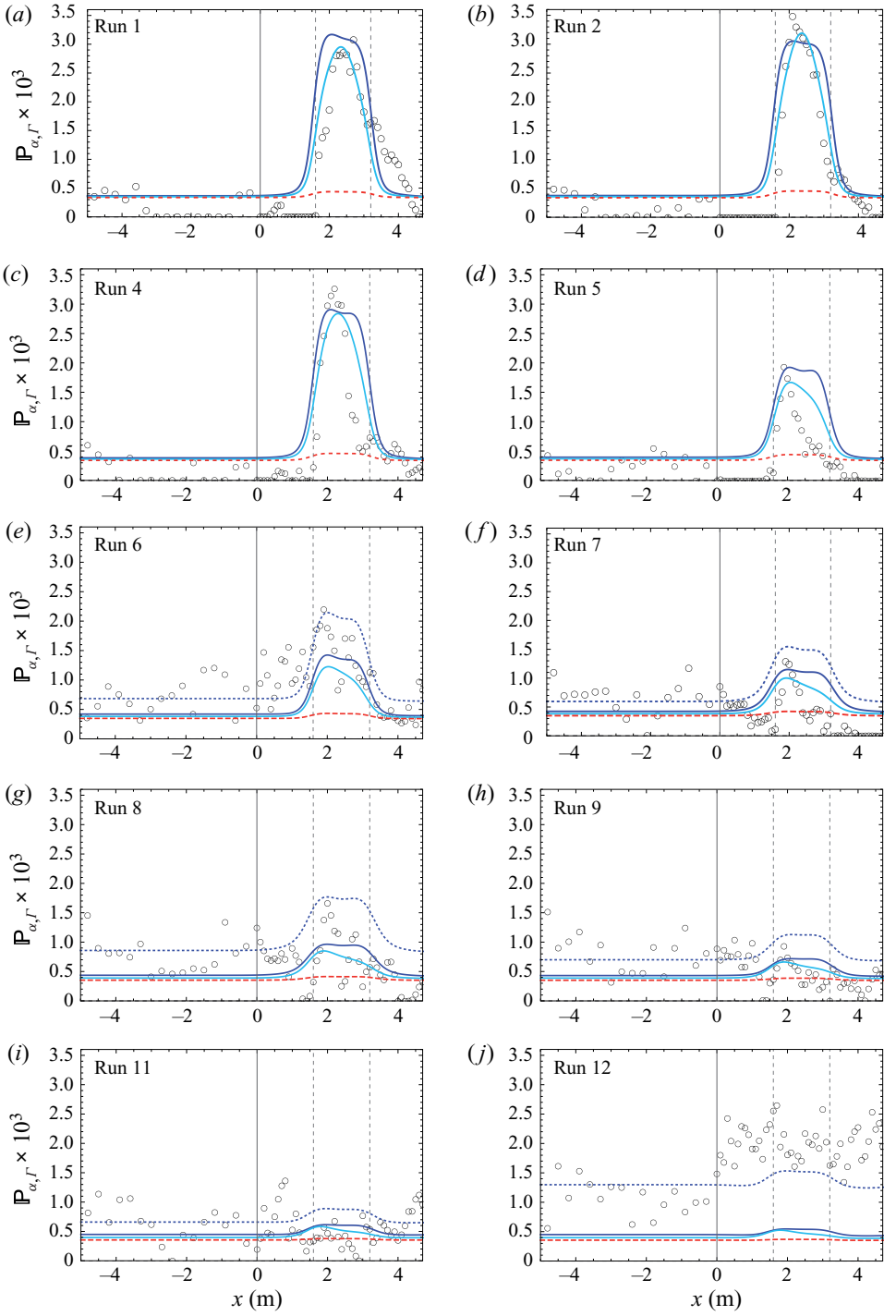

Figure 5. Evolution of the probability of rogue waves ($\alpha \geq 2$) over a shoal for Runs 1–2, 4–9, 11–12 from figure 5.8 of Raustøl (2014). Blue: model of (3.23) for a pre-shoal ($x < 0$) Rayleigh distribution with $\mathfrak{S}_0 = 1.2$. Cyan: same model, considering the evolution of skewness over the shoal. Dotted: model of (3.23) for a pre-shoal probability matched to the experimental data. Dashed: same as blue, but for symmetrical seas, $\mathfrak{S}_0 = 1$.

shallower region. Notably, Li *et al.* (2021*c*) have used a more general treatment for the surface elevation, containing both super- and sub-harmonics, as well as free and bound waves. Moreover, instead of bound super-harmonics in our model, one could investigate the effect of the nonlinear evolution of interacting free modes. For instance, similar experimental results were interpreted using a statistical matching of Korteweg–De Vries equilibrium states at the depth transition point (Majda *et al.* 2019; Moore *et al.* 2020). In retrospect to the ideas in Onorato & Suret (2016), these works obtained a connection between variance and skeweness with the dynamics. Therefore, subsequent investigations carrying out a comparison between the two types (free and bound) of mode evolution will be of great relevance.

5. Conclusion

This work presented a connection between statistical distributions and the fluid mechanics of the second-order perturbation in non-homogeneous conditions, providing successfully a physical explanation for the rogue wave probability increase over a depth change (Raustøl 2014; Trulsen *et al.* 2020). We have shown that our model reproduces very well the experiments of Raustøl (2014) and Trulsen *et al.* (2020) regarding the probability distribution as a function of the distance from the wavemaker. Moreover, we showed that the significant steepness and dimensionless depth affect the validity, and assessed numerically the extent of the deviation from the assumption of homogeneity. Furthermore, instead of introducing new physics (Haver & Andersen 2000), our model has demonstrated that an effective theory arises by challenging the homogeneity assumption. Introducing the $H_{1/3}/\sigma$ ratio (Goda 1983), we have established that the deep water regime produces no significant amplification of the height distribution, whereas the transitional water within $0.5 < k_p h < 1.5$ provides strong amplification, and the shallow water regime decreases this large amplification to a level smaller than the initial stage in deep water.

Our model has been restricted to reformulating normalised moments up to the variance only. The evolution of either skewness or kurtosis as a function of the distance from the wavemaker (Trulsen *et al.* 2020) will be addressed in a subsequent work. On the other hand, we have shown that it is possible to fit the data without the application of either skewness or kurtosis, as they are 'symptoms' of the dynamics and not the cause (Stansell 2004; Christou & Ewans 2014; Cattrell *et al.* 2018). Since our model relies on relations between steepness, slope and bandwidth that might be affected by a rapid depth change, the empirical findings in Mendes *et al.* (2021) regarding vertical asymmetry have to be extended to the current setting for an exact formulation. Furthermore, the generalisation of this work to multidirectional spectra would be needed, since Ducrozet & Gouin (2017) suggest that such a configuration weakens the effect of a varying bathymetry. Whether rogue waves are enhanced in strong bathymetry changes throughout most oceans or regionally under suitable conditions is yet to be assessed.

Funding. S.M., M.B. and J.K. were supported by the Swiss National Science Foundation under grant 200020-175697. S.M. and A.S. were supported by the National Science Foundation under grant OCE-1558978.

Declaration of interests. The authors report no conflict of interest.

Author ORCIDs.
S. Mendes https://orcid.org/0000-0003-2395-781X;
A. Scotti https://orcid.org/0000-0001-8283-3070;
M. Brunetti https://orcid.org/0000-0001-8199-223X;
J. Kasparian https://orcid.org/0000-0003-2398-3882.

Appendix A. Spectral analysis of spatial and temporal series

Below, we discuss two aspects of the assumptions necessary to obtain a sea with Gaussian statistics, the first dealing with a steady-state treatment of the statistical moments, and the second dealing with otherwise out-of-equilibrium conditions. First, we highlight that typically, classical definitions exhibit steady-state series as stationary and homogeneous in regard to translations in time and space, respectively. Traditionally, the Khintchine (1934) theorem is often written for the time domain, but it can be generalised to the spatial domain (Ripley 1981; Sherman 2010). Indeed, the spatial Khintchine theorem has the same structure, only replacing the time lag τ by a displacement vector $|\boldsymbol{\xi}| = \xi$ (Shinozuka & Jan 1972; Deodatis & Shinozuka 1988; Shinozuka & Deodatis 1988). For mean-ergodic homogeneous processes, the autocorrelation of the sea surface elevation (here, the surface elevation $\zeta(x, t)$ has been denoted as $\zeta(x)$ to ease the notation) can be computed properly from the spatial average $\langle\cdot\rangle_x$ as

$$\left.\begin{aligned} R_x(\xi) &:= \mathbb{E}[\zeta(x)\,\zeta(x+\xi)] = \langle \zeta(x)\,\zeta(x+\xi)\rangle_x, \\ \therefore \quad R_x(0) &\equiv \langle \zeta^2\rangle_x = \lim_{L\to+\infty} \frac{1}{L}\int_0^L \zeta^2(x)\,\mathrm{d}x, \end{aligned}\right\} \tag{A1}$$

such that one can find (Boccotti 2000; Goda 2010)

$$R_x(\xi) = \tfrac{1}{2}\sum_i a_i^2 \cos(k_i\xi), \quad \therefore \quad R_x(0) = \langle\zeta^2\rangle_x = \tfrac{1}{2}\sum_i a_i^2 = \mathscr{E}_{AIRY}. \tag{A2}$$

Moreover, in a mean-ergodic stationary time series, the ensemble average is computed exactly from the time average $\langle\cdot\rangle_t$, i.e. $R_t(\tau = 0) = \langle\zeta^2\rangle_t = \sum_i a_i^2/2$. Therefore, if a sufficiently large spatiotemporal series with uniform distribution of phases is ergodic, homogeneous in space and stationary in time, then we have

$$\mathbb{E}[\zeta] = \langle\zeta\rangle_x = \langle\zeta\rangle_t = 0, \quad \mathbb{E}[\zeta^2] = \langle\zeta^2\rangle_x = \langle\zeta^2\rangle_t = \tfrac{1}{2}\sum_i a_i^2, \tag{A3a,b}$$

thus narrowing down the possible solutions into the Gaussian distribution of the surface elevation because $\mathbb{E}[\zeta^{2n+1}] = 0$ for all $n \in \mathbb{N}$ and vanishing excess kurtosis. This procedure is very common in complex physical systems, and the above property is called ergodicity (Boltzmann 1898), while proving its validity is always a challenging task (Penrose 1973). The exact computation of the ensemble average of the sea surface elevation at an instant of time t_0 is not trivial (Goda 2010). Without ergodicity, the probability density of the surface elevation is unknown unless one assumes its expected value

$$\mathbb{E}[\zeta] = \int \zeta\,\mathrm{d}\mu(\zeta), \tag{A4}$$

where $\mathrm{d}\mu(\zeta)$ is a measure on the space of possible surface elevations. For an oscillatory system, it is customary to write $\zeta = r\cos(\phi)$ and introduce a joint p.d.f. on the space $[0, \infty) \times [0, 2\pi)$ that describes the statistical distribution of amplitudes and phases. Without loss of generality, we can always choose units in which $\mathbb{E}[\zeta^2] = 1$, and write

$$\text{p.d.f.} = \frac{f(r,\phi)}{2\pi}\, r\,\mathrm{e}^{-r^2/2}\,\mathrm{d}r\,\mathrm{d}\phi. \tag{A5}$$

The distribution of Longuet-Higgins (1952) is recovered if we assume that the phases are distributed uniformly and uncorrelated from the amplitudes, that is, $f(r, \phi) = 1$ (Rice

1945; Cramér & Leadbetter 1967; Mori & Yasuda 2002; Onorato *et al.* 2013). However, the uniform distribution of phases is appropriate only for narrow-banded signals (Davenport & Root 1987; Middleton 1996). For more realistic sea states, Tayfun (2008) shows that the p.d.f. introduced above should be corrected to account for correlations between phase and amplitude. As a first approximation, the correction proposed by Tayfun (2008) is

$$f(r,\phi) = 1 + \frac{\mu_3}{6} r(r^2 - 4)\cos\phi, \tag{A6}$$

where μ_3 is the skewness. Note that within this approximation, the expected value of even-order powers of ζ are not modified relative to the uniform phase approximation. Odd-order powers, which are zero when $f = 1$, are now non-zero. On the other hand, it is known that the weakly nonlinear evolution of a sea state which at $t = 0$ has random and uniformly distributed independent phases, remains so over the nonlinear time interval $t \gtrsim 2\pi/\omega_p$ (Choi, Lvov & Nazarenko 2004, 2005). Therefore, the source of correlations between phases and amplitudes cannot be attributed to the internal weakly nonlinear dynamics. However, this does not preclude that external factors (e.g. wind forcing) inducing non-equilibrium dynamics can nudge the phase distribution away from uniformity and/or impart a correlation between phases and amplitudes.

For the purpose of illustration, let us analyse the simplest effect of a uniform distribution. Through a change of variables (Papoulis 2002) and the law of the unconscious statistician (Blitzstein & Hwang 2019), we rewrite the ensemble average as

$$\mathbb{E}[\zeta] = \int_{-\infty}^{+\infty} \zeta f(\zeta)\,\mathrm{d}\zeta = \int_0^{2\pi} \zeta(\phi) f(\phi)\,\mathrm{d}\phi. \tag{A7}$$

Therefore, the uniform distribution of phases leads to ergodicity:

$$\mathbb{E}[\zeta] = \sum_i \frac{a_i}{2\pi}\int_0^{2\pi} \cos\phi\,\mathrm{d}\phi = \langle\zeta(x)\rangle = \lim_{L\to+\infty}\sum_i \frac{a_i}{L}\int_0^L \cos(k_i x)\,\mathrm{d}x = 0, \tag{A8}$$

$$\mathbb{E}[\zeta^2] = \sum_i \frac{a_i^2}{2\pi}\int_0^{2\pi} \cos^2\phi\,\mathrm{d}\phi = \langle\zeta^2(x)\rangle = \lim_{L\to+\infty}\sum_i \frac{a_i^2}{L}\int_0^L \cos^2(k_i x)\,\mathrm{d}x = \sum_i \frac{a_i^2}{2}. \tag{A9}$$

If we assume that correlations develop between the phases, then a weak departure from ergodicity will be observed. Below we show that due to the ergodicity assumption, the accuracy of Gaussian statistics will deteriorate, the narrower the superposition distribution. For the sake of measuring appreciable deviations and without loss of generality, we use a Boltzmann-like distribution, such that the ensemble average of the sea surface reads

$$\mathbb{E}^{(B)}[\zeta] = \sum_i \left[\frac{a_i}{\pi}\int_0^{+\infty} \frac{\cos\phi}{\mathrm{e}^{\phi/\pi}}\,\mathrm{d}\phi\right] = \sum_i \frac{a_i}{(1+\pi^2)} \sim 0.2\sqrt{m_0}, \tag{A10}$$

which is relatively small compared to the second moment of the surface elevation. For a tentative Gaussian-shaped superposition, however, one finds

$$\mathbb{E}^{(G)}[\zeta] \approx \sum_i a_i \left[\frac{3}{5}\int_0^{+\infty} \cos\phi\,\mathrm{e}^{-(\phi-1)^2}\,\mathrm{d}\phi\right] = \sum_i \frac{3a_i}{8} \sim 0.8\sqrt{m_0}, \tag{A11}$$

while for the square of the surface elevation we obtain

$$\mathbb{E}^{(B)}[\zeta^2] \approx \sum_i \frac{a_i^2}{\pi} \int_0^{+\infty} \mathrm{e}^{-\phi/\pi} \cos^2\phi \,\mathrm{d}\phi + \sum_{i\neq j} \frac{a_i a_j}{\pi} \int_0^{+\infty} \mathrm{e}^{-\phi/\pi} \cos\phi \,\mathrm{d}\phi$$
$$\approx \left(\frac{1+2\pi^2}{1+4\pi^2}\right) \sum_i a_i^2 + \sum_{i\neq j} \frac{a_i a_j}{1+\pi^2} \sim \left(\frac{4+14\pi^2+4\pi^4}{1+5\pi^2+4\pi^4}\right) m_0 \sim 1.2 m_0. \tag{A12}$$

Lacking a closed form, the Gaussian-like distribution of phases reads, instead,

$$\mathbb{E}^{(G)}[\zeta^2] \approx \sum_i \frac{5a_i^2}{13} + \sum_{i\neq j} \frac{3a_i a_j}{8} \sim 1.53 m_0. \tag{A13}$$

Comparing the deviations from the uniform superposition in (A10)–(A12) gives

$$\delta\mathbb{E}_{1,2}^{(B)} = \frac{\sqrt{\mathbb{E}^{(B)}[\zeta^2] - \mathbb{E}^{(U)}[\zeta^2]}}{\mathbb{E}^{(B)}[\zeta] - \mathbb{E}^{(U)}[\zeta]} = \frac{\sqrt{1.2m_0 - m_0}}{0.2\sqrt{m_0} - 0} \approx 2.3, \tag{A14}$$

whereas for the Gaussian one we have

$$\delta\mathbb{E}_{1,2}^{(G)} = \frac{\sqrt{\mathbb{E}^{(G)}[\zeta^2] - \mathbb{E}^{(U)}[\zeta^2]}}{\mathbb{E}^{(G)}[\zeta] - \mathbb{E}^{(U)}[\zeta]} = \frac{\sqrt{1.53m_0 - m_0}}{0.8\sqrt{m_0} - 0} \approx 0.9, \tag{A15}$$

implying a decreasing gap between moments when the superposition distribution is narrower. In these examples, we see that even the linear evolution of a sea state that at some point in time has a non-uniform distribution of phases breaks ergodicity. We remark that the break in ergodicity and being Gaussian are not necessarily simultaneous, as in the above case.

Appendix B. Energetic formulae derivation

Given (3.6) and taking the limit of very large number of amplitude components towards an asymptotic leading order, the energy computation is reduced to the coefficients $(\Omega_m, \tilde{\Omega}_m)$. Then, having $u_i = \partial\Phi/\partial x_i$ and using the notation $I = u_1^2 + u_3^2$, one obtains

$$I = \left[\frac{\partial}{\partial x}\left\{\sum_j f_j \cosh(j\varphi)\sin(j\phi)\right\}\right]^2 + \left[\frac{\partial}{\partial z}\left\{\sum_j f_j \cosh(j\varphi)\sin(j\phi)\right\}\right]^2$$
$$= \left[\sum_j jk \times f_j \cosh(j\varphi)\cos(j\phi)\right]^2 + \left[\sum_j jk \times f_j \sinh(j\varphi)\sin(j\phi)\right]^2$$
$$= \left[\sum_m \Omega_m \cosh(m\varphi)\cos(m\phi)\right]\left[\sum_n \Omega_n \cosh(n\varphi)\cos(n\phi)\right]$$
$$+ \left[\sum_m \Omega_m \sinh(m\varphi)\sin(m\phi)\right]\left[\sum_n \Omega_n \sinh(n\varphi)\sin(n\phi)\right], \tag{B1}$$

where we defined $\Omega_m = mkf_m$ and estimated the effect of $|\partial h/\partial x|$ to not be of leading order for this sum (see §§ 3 and 4.2). By means of the notation

$$\mathfrak{Cos}_{mn}(\varphi, \phi) := \cosh(m\varphi) \times \cos(n\phi); \quad \mathfrak{Sin}_{mn}(\varphi, \phi) := \sinh(m\varphi) \times \sin(n\phi), \tag{B2a,b}$$

the algebra yields

$$\begin{aligned} I &= \sum_{m=n} \Omega_m^2 \, \mathfrak{Cos}_{mm}^2(\varphi, \phi) + \sum_{m \neq n} \Omega_m \Omega_n \, \mathfrak{Cos}_{mm}(\varphi, \phi) \, \mathfrak{Cos}_{nn}(\varphi, \phi) \\ &\quad + \sum_{m=n} \Omega_m^2 \, \mathfrak{Sin}_{mm}^2(\varphi, \phi) + \sum_{m \neq n} \Omega_m \Omega_n \, \mathfrak{Sin}_{mm}(\varphi, \phi) \, \mathfrak{Sin}_{nn}(\varphi, \phi) \\ &:= \sum_m \Omega_m^2 I_{mm} + \sum_{m \neq n} \Omega_m \Omega_n I_{mn}. \end{aligned} \tag{B3}$$

However, one can further expand the trigonometric clusters in (B2) as follows:

$$\begin{aligned} 4I_{mn} &= 4 \, \mathfrak{Cos}_{mm}(\varphi, \phi) \, \mathfrak{Cos}_{nn}(\varphi, \phi) + 4 \, \mathfrak{Sin}_{mm}(\varphi, \phi) \, \mathfrak{Sin}_{nn}(\varphi, \phi) \\ &= [\cos(m\phi)\cos(n\phi) + \sin(m\phi)\sin(n\phi)] \times 2\cosh[(m+n)\varphi] \\ &\quad + [\cos(m\phi)\cos(n\phi) - \sin(m\phi)\sin(n\phi)] \times 2\cosh[(m-n)\varphi] \\ &= 2\cosh[(m+n)\varphi]\cos[(m-n)\phi] + 2\cosh[(m-n)\varphi]\cos[(m+n)\phi]. \end{aligned} \tag{B4}$$

As an immediate corollary, we find $2I_{mm} = \cosh(2m\varphi) + \cos(2m\phi)$. Using the algebra from (B4) and periodic integration, following the expression for the energy in (2.4) and subtracting the potential energy $\rho g h_0^2/2$ due to the water column, we find in the limit $i \to \infty$ the leading-order energy density

$$\mathscr{E} \approx \sum_m \frac{\tilde{\Omega}_m^2}{4} + \sum_m \frac{\Omega_m^2}{4g} \int_{-h}^{0} \cosh(2m\varphi) \, \mathrm{d}z \approx \frac{1}{4} \sum_m \left[\tilde{\Omega}_m^2 + \Omega_m^2 \, \frac{\sinh(2mkh)}{2mgk} \right]. \tag{B5}$$

As we assumed a small effect of $\partial h/\partial x$ in the previous integral, the bathymetry will appear in $\varphi = k(z+h)$ as well as in Ω_m and $\tilde{\Omega}_m$. Likewise, using the definition of (3.6), and taking into account the discussion in (3.2) and (3.3), we compute the time average of the squared sea surface elevation at a fixed point $x_i \in \mathbb{R}$:

$$\langle \zeta^2 \rangle_t = \lim_{T \to +\infty} \frac{1}{T} \int_0^T \left[\sum_m \tilde{\Omega}_m \cos(m\phi) \right] \left[\sum_n \tilde{\Omega}_n \cos(n\phi) \right] \mathrm{d}t = \sum_m \frac{\tilde{\Omega}_m^2}{2}, \tag{B6}$$

where the function $\tilde{\Omega}_m = \tilde{\Omega}_m(x)$ is also a function of x due to its dependence on significant steepness $\varepsilon = \varepsilon(x)$ and dimensionless depth $k_p h = (k_p h)(x)$. To compare the generalised model with the specific case of Airy's solution, we set $m = 1$. In this case, $\tilde{\Omega}_1 = a$ while $\Omega_1 = agk/\omega \cosh kh$ (Dingemans 1997), the dispersion relation is expressed as $\omega^2 = gk \tanh kh$, so that the spatial energy density is

$$\begin{aligned} \mathscr{E}_1 &= \frac{1}{4} \left[a^2 + \left(\frac{agk}{\omega \cosh kh} \right)^2 \frac{\sinh(2kh)}{2gk} \right] \\ &= \frac{1}{4} \left[a^2 + \left(\frac{a^2 g^2 k^2}{gk \tanh kh \times \cosh^2 kh} \right) \frac{2 \sinh kh \cosh kh}{2gk} \right] = \frac{a^2}{2}, \end{aligned} \tag{B7}$$

thus recovering the spatial energy density in (2.6). For the second order, we have

$$\Omega_1 = \frac{a\omega}{\sinh kh}, \quad \Omega_2 = \frac{3ka^2\omega}{4\sinh^4 kh}, \quad \tilde{\Omega}_1 = a, \quad \tilde{\Omega}_2 = \frac{ka^2\cosh kh}{4\sinh^3 kh}\left[2+\cosh(2kh)\right]. \tag{B8a–d}$$

Upon the steepness being expressed as $ka = (2\pi/\lambda)\times(H/2) = \pi\varepsilon$, the spatial energy density is computed and leads to (3.10*a*,*b*)–(3.11*a*,*b*):

$$\begin{aligned}\mathscr{E}_2 &= \frac{a^2}{2} + \frac{1}{4}\left\{\frac{k^2a^4}{16}\left[\frac{\cosh kh}{\sinh^3 kh}\left(2+\cosh(2kh)\right)\right]^2 + \left(\frac{3ka^2\omega}{4\sinh^4 kh}\right)^2\frac{\sinh(4kh)}{4gk}\right\}\\ &= \frac{a^2}{4}\left\{2+\left(\frac{\pi\varepsilon}{4}\right)^2\left[\frac{\cosh kh}{\sinh^3 kh}\left(2+\cosh(2kh)\right)\right]^2 + \left(\frac{\pi\varepsilon}{4}\right)^2\left[\frac{9\cosh(2kh)}{\sinh^6 kh}\right]\right\}.\end{aligned} \tag{B9}$$

Appendix C. Amplification universality

Here we will prove the validity of the two relations in (3.23). The result in (3.23) assures us of the invariance of the ratio of logarithms in (3.21) and the amplification (ratio of probabilities) in (3.22), regardless of the equilibrium exceedance probability prior to the shoal. Let us set up a general expression to accommodate both super-Rayleigh (+) and sub-Rayleigh (−) distributions, e.g. those that assign higher or lower probabilities than prescribed by Longuet-Higgins (1952) at either the bulk or tail of the distribution. We attach a factor $g^{\pm}_{\mu\alpha}$ to the Rayleigh distribution, denoting a Gram–Charlier (GC) series (Longuet-Higgins 1963; Mori & Yasuda 2002). Equation (3.23) holds if one can prove that the variance is corrected by a negligible term, denoted by $\mathfrak{L}_\mu$:

$$\mathbb{P}^{\pm}_{\alpha,\mu} = g^{\pm}_{\mu\alpha}\times\mathcal{R}_\alpha, \quad \therefore \quad \mathbb{P}^{\pm}_{\alpha,\mu}(\Gamma) = \left(\mathbb{P}^{\pm}_{\alpha,\mu}\right)^{1/\Gamma\pm\mathfrak{L}_\mu} = \left(g^{\pm}_{\mu\alpha}\,\mathrm{e}^{-2\alpha^2}\right)^{1/\Gamma\pm\mathfrak{L}_\mu}. \tag{C1}$$

We will show that this term satisfies $\mathfrak{L}_\mu \ll \Gamma$. Without loss of generality, the dual GC-ζ distribution with $|\mu_3| = |\mu_4| = 1/2$ reads (Mori & Yasuda 2002)

$$f^{\pm}_{\mu}(\zeta) \equiv f_\zeta(m_0)\times g^{\pm}_{\mu\zeta} = \frac{\mathrm{e}^{-\zeta^2/2m_0}}{\sqrt{2\pi m_0}}\left[1\pm\frac{1}{12}(\zeta^3-3\zeta)\pm\frac{1}{48}(\zeta^4-6\zeta^2+3)\right]. \tag{C2}$$

Clearly, the term $g^{\pm}_{\mu\alpha}$ is a by-product of the surface elevation counterpart $g^{\pm}_{\mu\zeta}$. Hence the following model captures the features of the two non-Gaussian distributions while being properly normalised:

$$\frac{16}{16\mp(\Gamma-1)^2}\int_{-\infty}^{+\infty} f_\zeta(m_0\Gamma)\times g^{\pm}_{\mu\zeta}\,\mathrm{d}\zeta = \int_{-\infty}^{+\infty} f^{\pm}_{\mu}(\zeta,\Gamma)\,\mathrm{d}\zeta = 1. \tag{C3}$$

The first normalised moments read (see figure 6)

$$\mu_1^{\pm} = \int_{-\infty}^{+\infty}\frac{16g^{\pm}_{\mu\zeta}f_\zeta(\Gamma)\,\zeta}{16\mp(\Gamma-1)^2}\,\mathrm{d}\zeta = \pm\frac{4\Gamma(\Gamma-1)}{\left[16\mp(\Gamma-1)^2\right]}, \tag{C4}$$

while the sub-Rayleigh second normalised moment is expressed as

$$\mu_2^{-} = \int_{-\infty}^{+\infty}\frac{16g^{-}_{\mu\zeta}f_\zeta(\Gamma)\,(\zeta-\mu_1^-)^2}{16+(\Gamma-1)^2}\,\mathrm{d}\zeta = \Gamma\left[1+\frac{4\Gamma^4-28\Gamma^3-20\Gamma^2+44\Gamma}{\left(15+2\Gamma-\Gamma^2\right)^2}\right], \tag{C5}$$

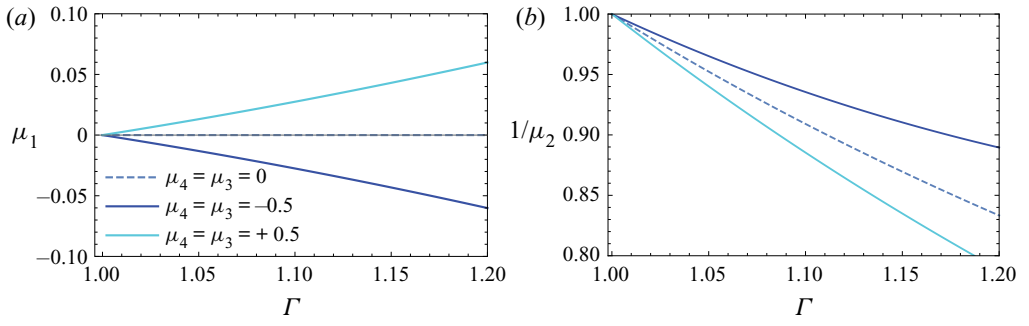

Figure 6. Γ-GC model: (*a*) ensemble average of the surface elevation; (*b*) its variance.

and the super-Rayleigh (see figure 6) as

$$\mu_2^+ = \int_{-\infty}^{+\infty} \frac{16 g_{\mu\zeta}^+ f_\zeta(\Gamma)\,(\zeta - \mu_1^+)^2}{16 - (\Gamma - 1)^2}\,\mathrm{d}\zeta = \Gamma\left[1 + \frac{4\Gamma^4 - 28\Gamma^3 + 108\Gamma^2 - 84\Gamma}{\left(17 - 2\Gamma + \Gamma^2\right)^2}\right]. \tag{C6}$$

Comparing the variances with the exponent in (C1), we find $\mu_2^\pm = \Gamma(1 \pm \mathfrak{L}_\mu/\Gamma)$, and the corrections $\mathfrak{L}_\mu$ can be available readily by isolating the quotients inside the brackets of the right-hand sides of the above equations. These coefficients can be further approximated (recalling that $|\Gamma - 1| \ll 1$) as

$$|\mu_1^\pm| \approx \frac{(\Gamma - 1)}{4}, \quad \mu_2^\pm \approx \Gamma \pm \frac{(\Gamma - 1)}{3}. \tag{C7a,b}$$

Then we showed a weak proof of the first part of (3.23) by demonstrating that a change $g_{\mu\alpha}^\pm$ in the pre-shoal Rayleigh probability will always be met by a change $\pm\mathfrak{L}_\mu$ in the variance, typically obeying $\mathfrak{L}_\mu/\Gamma \ll 1$ (see figure 6*b*).

C.1. *Generalised proof*

In this subsection, we use the Γ-GC model to obtain exact closed-form wave height distributions, following the steps for the integration of the envelope in a two-dimensional random walk of Mori & Yasuda (2002). Thus we integrate the joint distribution of both surface elevation ζ and its Hilbert transform $\tilde{\zeta}$ over the uniform distribution of phases, obtaining the marginal density of the surface envelope:

$$f_{\mu,R}^\pm(\Gamma) = \int_0^{2\pi} g_{\mu\zeta}^\pm f_\zeta^\pm(\Gamma) \times g_{\mu\tilde{\zeta}}^\pm f_{\tilde{\zeta}}^\pm(\Gamma)\, R\,\mathrm{d}\phi, \tag{C8}$$

where $\sqrt{\zeta^2 + \tilde{\zeta}^2} = R$ is the envelope with $\zeta = R\cos\phi$ and $\tilde{\zeta} = R\sin\phi$. Performing this integration, changing variables to wave heights and later normalising by $H_{1/3} = 4m_0 = 4$

and integrating again as in (2.2), we find (see figures 7*a*,*b*)

$$\mathbb{P}^{\pm}_{\alpha,\mu}(\Gamma) = \frac{\mathrm{e}^{-2\alpha^2/\Gamma}}{3}\left[1 + \frac{2\alpha^8 + 4\alpha^6(\Gamma-4) + 6\alpha^4(\Gamma^2 - 4\Gamma + 6 \pm 32)}{[16 \mp (\Gamma-1)^2]^2} + \frac{3\alpha^2(\Gamma-2)(\Gamma^2 - 2\Gamma + 2 \pm 32)}{[16 \mp (\Gamma-1)^2]^2}\right]. \tag{C9}$$

Then, in analogy with (3.21), we are able to assess whether the proposition in (C1) holds by verifying the ratio

$$\frac{\ln\left[\mathbb{P}^{\pm}_{\alpha,\mu}\right]}{(\Gamma \pm \mathfrak{L}_\mu)\ln\left[\mathbb{P}^{\pm}_{\alpha,\mu}(\Gamma)\right]} = 1, \quad \therefore \quad \frac{\ln\left[\mathbb{P}^{\pm}_{\alpha,\mu}\right]}{\Gamma\ln\left[\mathbb{P}^{\pm}_{\alpha,\mu}(\Gamma)\right]} = 1 \pm \frac{\mathfrak{L}_\mu}{\Gamma} \approx 1. \tag{C10}$$

Accordingly, figures 7(*c*,*d*) display the magnitude of the correction $1 \pm \mathfrak{L}_\mu/\Gamma$ in the variance. When $\Gamma \approx 1.15$, we see that super-Rayleigh distributions have a maximal 4 % increase in the variance Γ, whereas sub-Rayleigh distributions exhibit the opposite but of smaller magnitude, confirming the estimates in the weak proof. As the validity of (C1) has been demonstrated, one can prove the universality of the amplification regardless of the distribution, i.e. extend (3.22) to an arbitrary distribution. Having in mind the order of magnitude of $\mathfrak{L}_\mu/\Gamma$, we can rewrite (C1) (defining $|\ln g^{\pm}_{\mu\alpha}| = \ln g_{\mu\alpha}$) as

$$\mathbb{P}^{\pm}_{\alpha,\mu}(\Gamma) = (\exp(-2\alpha^2 \pm \ln g_{\mu\alpha}))^{1/\Gamma \pm \mathfrak{L}_\mu} \approx \exp\left[-\frac{2\alpha^2}{\Gamma}\left(1 \mp \frac{\ln g_{\mu\alpha}}{2\alpha^2}\right)\left(1 \mp \frac{\mathfrak{L}_\mu}{\Gamma}\right)\right]. \tag{C11}$$

Furthermore, the relative probability becomes

$$\begin{aligned}
\frac{\mathbb{P}^{\pm}_{\alpha,\mu}(\Gamma)}{\mathbb{P}^{\pm}_{\alpha,\mu}} &= \exp\left[(-2\alpha^2 \pm \ln g_{\mu\alpha})\left(\frac{1}{\Gamma \pm \mathfrak{L}_\mu} - 1\right)\right] \\
&= \exp\left[2\alpha^2\left(1 \mp \frac{\ln g_{\mu\alpha}}{2\alpha^2}\right)\left(1 - \frac{1}{\Gamma \pm \mathfrak{L}_\mu}\right)\right] \\
&= \exp\left[2\alpha^2\left(1 - \frac{1}{\Gamma}\right)\left(1 \mp \frac{\ln g_{\mu\alpha}}{2\alpha^2}\right)\left(1 \pm \frac{\mathfrak{L}_\mu}{\Gamma^2\left(1 - \frac{1}{\Gamma}\right)}\right)\right] \\
&= \exp\left[2\alpha^2\left(1 - \frac{1}{\Gamma}\right)\left(1 \mp \frac{\ln g_{\mu\alpha}}{2\alpha^2}\right)\left(1 \pm \frac{\mathfrak{L}_\mu}{\Gamma\,(\Gamma-1)}\right)\right] \\
&\equiv \exp\left[2\alpha^2\left(1 - \frac{1}{\Gamma}\right)(1 \mp \delta_{\mu\alpha})(1 \pm \delta_{\mu\Gamma})\right].
\end{aligned} \tag{C12}$$

As $|\Gamma - 1| \ll 1$, it is straightforward to see that $\delta_{\mu\Gamma} = \mathfrak{L}_\mu/\Gamma(\Gamma-1) \sim 10\mathfrak{L}_\mu \sim \delta_{\mu\alpha} = (\ln g_{\mu\alpha})/2\alpha^2$, plotted for comparison in figure 8. Hence we conclude that for the probability amplification, the second correction term $\delta_{\mu\Gamma}$ counters $\delta_{\mu\alpha}$. Thus we have proved the first-order amplification universality with $\mu_3 \sim \mu_4 < 1$:

$$\begin{aligned}
\frac{\mathbb{P}^{\pm}_{\alpha,\mu}(\Gamma)}{\mathbb{P}^{\pm}_{\alpha,\mu}} &= \exp\left(2\alpha^2\left(1 - \frac{1}{\Gamma}\right) \pm O(\Gamma - 1)\right) \\
&\approx \exp\left(2\alpha^2\left(1 - \frac{1}{\Gamma}\right)\right) \equiv \frac{\mathcal{R}_\alpha(\Gamma)}{\mathcal{R}_\alpha}, \quad \forall\, g^{\pm}_{\mu\alpha} \in \mathbb{R}_+.
\end{aligned} \tag{C13}$$

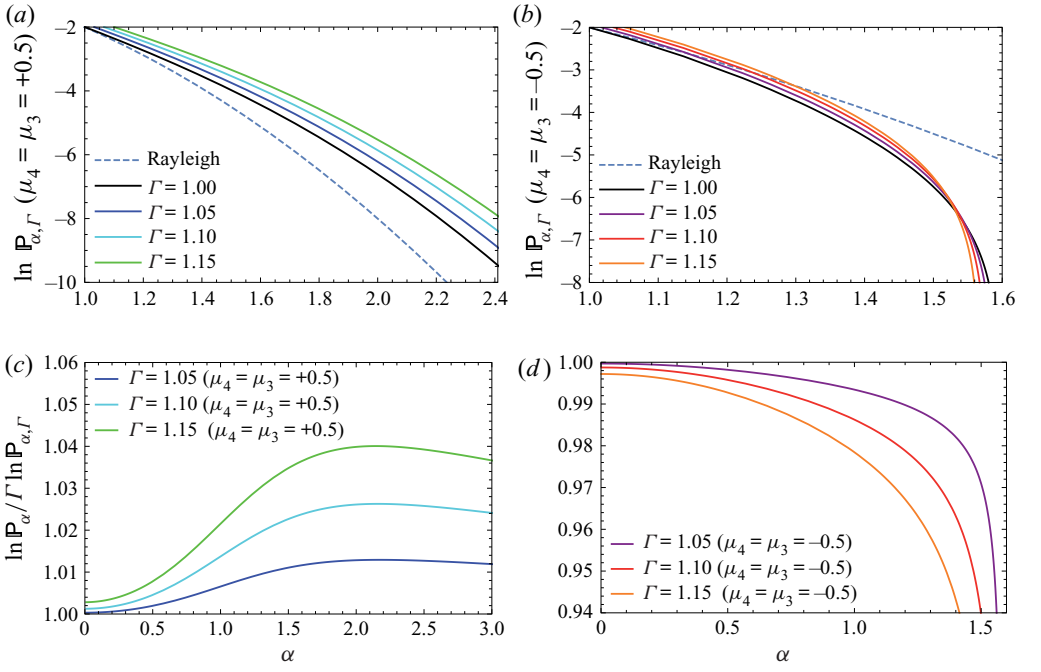

Figure 7. Γ-GC probability distribution for: (*a*) super-Rayleigh and (*b*) sub-Rayleigh. The correction to (3.21) through $\mathfrak{L}_\mu$ in (C10) is found for (*c*) super-Rayleigh and (*d*) sub-Rayleigh regimes.

Rogue waves in (3.24) have $2\alpha^2[1-(\mathfrak{S}_0^2\Gamma)^{-1}]\leqslant 3$, resulting in maximal correction $\mathrm{e}^{\mathcal{O}(\Gamma-1)}\approx \mathrm{e}^{3\times 0.03}<1.1$, suggesting an upper bound of 8–9 % variation from the universal amplification. On the other hand, figure 8 shows $(1\mp\delta_{\mu\alpha})(1\pm\delta_{\mu\Gamma})\approx 1.14$ for ordinary waves ($\alpha\leqslant 1$) instead of $(1\mp\delta_{\mu\alpha})(1\pm\delta_{\mu\Gamma})\leqslant 1.04$ for rogue waves, such that the main term of (3.24) becomes $2\alpha^2[1-(\mathfrak{S}_0^2\Gamma)^{-1}]\leqslant 1$, and the first-order correction reads $\mathrm{e}^{\mathcal{O}(\Gamma-1)}\approx \mathrm{e}^{0.6\times 0.15}<1.1$. Hence the bound is upheld by any normalised wave height.

Appendix D. Parameterisation generality and compact formulation

Under adequate conditions of $Ur\leqslant 8\pi^2/3$ (Dean & Dalrymple 1984) and for shoals in Regime II, (3.26) can be rewritten in a more compact form. First, however, let us demonstrate that (3.26) holds regardless of which reference steepness is chosen to compute κ_0. For relatively higher or lower reference steepness $\varepsilon_\pm=\langle\varepsilon\rangle\pm\delta\varepsilon$, we find

$$\kappa_0^\pm=\frac{\ln\left[\max\mathfrak{S}_0\right]}{\ln\left[\max\Gamma\left(\langle\varepsilon\rangle\pm\delta\varepsilon,k_ph,\mathfrak{S}_0\right)\right]}\approx\kappa_0\mp\delta\kappa_0, \tag{D1}$$

in turn affecting the probability amplification only marginally:

$$\left(\frac{\ln\mathbb{P}_\alpha}{\ln\mathbb{P}_{\alpha,\Gamma}}\right)_\pm=[\Gamma_0\pm\delta\Gamma_0]^{2\kappa_0\mp 2\delta\kappa_0}\times\Gamma\left(\varepsilon(x),k_ph(x),\mathfrak{S}_0\right)\approx\frac{\ln\mathbb{P}_\alpha}{\ln\mathbb{P}_{\alpha,\Gamma}}. \tag{D2}$$

This relation holds because the typical difference between the Γ correction atop the shoal and the average moving during the shoal does not exceed $\delta\Gamma_0/\Gamma_0\leqslant 2\,\%$. We corroborate

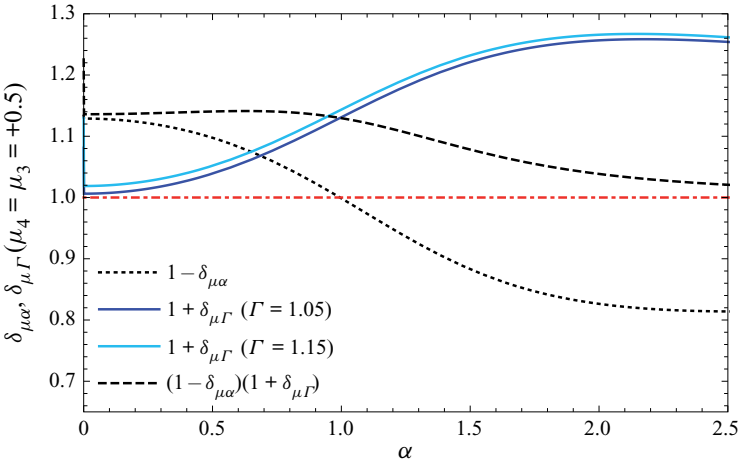

Figure 8. Comparison between first-order corrections to the amplification of the Γ-GC exceedance probability for positive skewness and kurtosis as in (C12).

this by comparing the equivalent of figure 5(*a*) for a 0.5 % higher Γ correction than its reference $\Gamma_0 = 1.031$ in figure 9(*a*). Considering that Run 1 had maximal correction $\Gamma \approx 1.041$, the choice for the reference κ_0 does not affect the validity of (3.26). To obtain a compact formulation of (3.26), we notice that at a fixed point in space, i.e. at a distance $x = x_i$ from the wavemaker, the asymmetry $\mathfrak{S}_0$ does not depend on how we plot Γ. Therefore, we can approximate

$$\mathfrak{S}_0(x = x_i) = \left[\Gamma\left(\varepsilon(x_i), k_p h(x_i), \mathfrak{S}_0\right)\right]^{\kappa_x} \approx \left[\Gamma\left(\langle\varepsilon\rangle, k_p h, \mathfrak{S}_0\right)\right]^{\kappa_0}, \quad \forall\, x_i \in \mathbb{R}. \tag{D3}$$

As the two versions of the Γ correction differ, as shown in figure 9(*b*), one concludes that $\kappa(k_p h) \equiv \kappa_0 \neq \kappa_x$. Thus we obtain

$$\ln \mathfrak{S}_0 \approx \langle\kappa_x\rangle \ln\langle\Gamma(x)\rangle \approx \kappa_0 \ln\left\langle\Gamma\left(\langle\varepsilon\rangle, k_p h, \mathfrak{S}_0\right)\right\rangle, \tag{D4}$$

whose Regime II restriction is translated numerically to $\Gamma \geqslant 1 + \mathcal{O}(g^{-2})$, leading to $\langle\kappa_x\rangle \approx 0.64\kappa_{kh}$, as shown in figure 9(*b*). Therefore, we can estimate conservatively throughout the entire trajectory:

$$\left[\Gamma\left(\langle\varepsilon\rangle, k_p h, \mathfrak{S}_0\right)\right]^{2\kappa_0} \approx \left[\Gamma\left(\varepsilon(x), k_p h(x), \mathfrak{S}_0\right)\right]^{1.2\kappa_0}. \tag{D5}$$

Thus the ratio of the probabilities is better estimated and greatly simplified as

$$\frac{\ln \mathbb{P}_\alpha}{\ln \mathbb{P}_{\alpha,\Gamma}} \approx \left[\Gamma\left(\varepsilon(x), k_p h(x), \mathfrak{S}_0\right)\right]^{1+1.2\kappa_0}. \tag{D6}$$

Appendix E. Analytical description of steepness and depth

In order to smooth as well as to facilitate the handling of the experimental data on wave steepness and dimensionless depth, we fitted them against analytic functions, as follows:

$$\begin{aligned}\varepsilon = {} & \varepsilon_1 + \varepsilon_2 \exp(-(x - 2.4)^4) + \varepsilon_3 \exp(-(2 + \delta_{31})[x - 1.4 + \delta_{32}]^2) \\ & + \varepsilon_4 \exp(-(1 + \delta_{41})[x - 4.9 + \delta_{42}]^2),\end{aligned} \tag{E1}$$

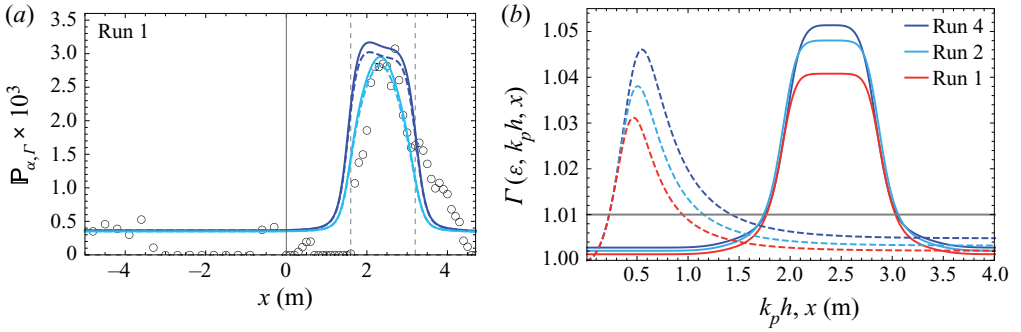

Figure 9. (*a*) Equivalent of figure 5(*a*) for a higher reference Γ correction due to steepness $\varepsilon_+ \approx 1.16\langle\varepsilon\rangle$ (dashed) and its original description according to (3.26) (solid). Notice that this 16 % increase in the reference steepness decreases the blue curve model by 4 % and the cyan one by 2 %. (*b*) Plot of Γ correction for Runs 1–4 of Raustøl (2014) as a function of dimensionless depth (dashed) and distance from the wavemaker (solid) with variables (ε, kh) modelled by Appendix E, whereas the minimum threshold applicable ($\Gamma \geqslant 1.01$) representative of Regime II is depicted by the thin horizontal line. The averages over these ranges read approximately $\langle\Gamma(x)\rangle = 1.036$ and $\langle\Gamma(k_p h)\rangle = 1.023$.

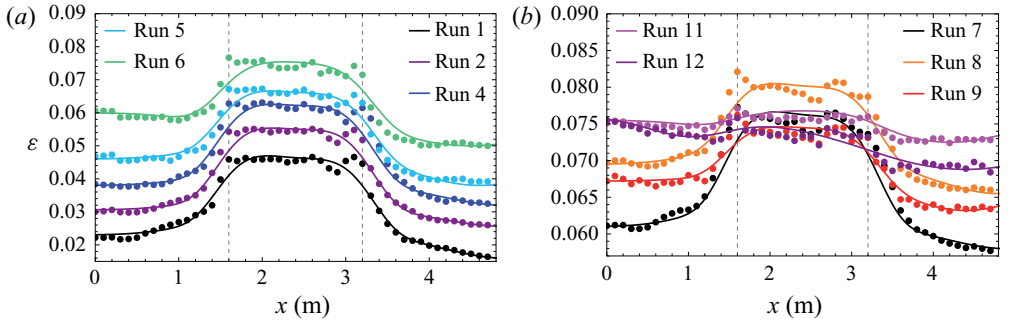

Figure 10. Modelling of the significant steepness in Raustøl (2014) experiments according to (E1), corrected to the term $\varepsilon = H_{1/3}/\bar{\lambda} = (4/\pi)k_p a_c$. Dots represent data extracted from figure 5.4 of Raustøl (2014). Vertical dashed lines depict the rising shoal end ($x = 1.6$) and beginning of the descending shoal ($x = 3.2$).

while the modelling for the depth is computed as

$$k_p h = D_1 + D_2 \exp(-0.25(x - 2.4)^4) + D_3 \exp(-2[x + \delta_{62} - 0.7]^2) + D_4 \exp(-2[x + \delta_{82} - 4.2]^2). \tag{E2}$$

The values of these coefficients for ten runs of Raustøl (2014) and Trulsen *et al.* (2020) are given in table 1. As displayed in figure 10, these fits provide an accurate description of the actual data. Re-scaled by $\pi/4$, the first steepness coefficient ε_1 is equal to the pre-shoal steepness in table 1 of Trulsen *et al.* (2020), while $\varepsilon_1 + \varepsilon_2$ is the shallower steepness of the shoal. Likewise, the coefficient D_1, which was extracted from Raustøl (2014) through the formula $k_p h \approx (\pi\varepsilon/4Ur)^{1/3}$ (see Trulsen *et al.* 2020), equals approximately the largest values of the dimensionless depth, while $D_1 + D_2$ recovers the smallest values. Note, however, that Trulsen *et al.* (2020) display the averages of each side, while we model every value according to the 16 probes of figure 2 in Trulsen *et al.* (2020).

Exp.	ε_1	ε_2	ε_3	ε_4	δ_{31}	δ_{32}	δ_{41}	δ_{42}	D_1	D_2	D_3	D_4	δ_{62}	δ_{82}
Run 1	0.0230	0.0230	0.0030	−0.0070	—	—	—	—	1.85	−1.32	−0.40	−0.50	—	—
Run 2	0.0306	0.0242	0.0020	−0.0050	—	—	—	—	2.08	−1.50	−0.45	−0.45	—	0.1
Run 4	0.0380	0.0240	0.0020	−0.0060	—	—	—	—	2.60	−1.93	−0.60	−0.60	—	0.1
Run 5	0.0460	0.0200	0.0020	−0.0080	—	—	—	0.3	3.20	−2.40	−0.80	−0.75	—	0.1
Run 6	0.0600	0.0167	−0.0020	−0.0100	—	—	−0.5	0.4	4.15	−3.20	−0.99	−0.99	−0.1	0.1
Run 7	0.0610	0.0150	0.0020	−0.0030	—	—	—	—	2.50	−1.50	−0.50	−0.50	−0.1	0.1
Run 8	0.0695	0.0105	0.0015	−0.0040	—	—	—	0.1	3.05	−2.00	−0.80	−0.80	—	0.1
Run 9	0.0672	0.0073	0.0005	−0.0040	—	—	—	0.5	3.40	−2.15	−0.55	−0.60	−0.1	0.1
Run 11	0.0755	0.0015	−0.0008	−0.0030	—	0.4	−0.5	0.7	4.30	−2.85	−0.85	−0.80	−0.1	0.1
Run 12	0.0760	0.0002	−0.0025	−0.0072	—	0.4	−0.7	0.5	4.95	−3.30	−1.00	−1.00	−0.1	0.1

Table 1. Summary of all coefficients for the modelling in (E1) and (E2).

References

Adak, S. 1995 *Time-Dependent Spectral Analysis of Nonstationary Time Series*. Stanford University.

Airy, G.B. 1845 Tides and waves. In *Encyclopaedia Metropolitana*, vol. 122, pp. 241–396. B. Fellowes.

Alkhalidi, M.A. & Tayfun, M.A. 2013 Generalized Boccotti distribution for nonlinear wave heights. *Ocean Engng* **74**, 101–106.

Barbariol, F., Benetazzo, A., Carniel, S. & Sclavo, M. 2015 Space-time wave extremes: the role of metocean forcings. *J. Phys. Oceanogr.* **45** (7), 1897–1916.

Benjamin, T.B. & Feir, J.E. 1967 The disintegration of wave trains on deep water. Part 1. Theory. *J. Fluid Mech.* **27** (3), 417–430.

Blitzstein, J.K. & Hwang, J. 2019 *Introduction to Probability*, 2nd edn. CRC Press, Taylor & Francis Group.

Boccotti, P. 2000 *Wave Mechanics for Ocean Engineering*. Elsevier Oceanography Series. Elsevier.

Bolles, C.T., Speer, K. & Moore, M.N.J. 2019 Anomalous wave statistics induced by abrupt depth change. *Phys. Rev. Fluids* **4** (1), 011801(R).

Boltzmann, L. 1898 *Vorlesungen für Gastheorie, II. Teil*. J. A. Barth.

Bruscato, A. & Toloi, C.M. 2004 Spectral analysis of non-stationary processes using the Fourier transform. *Braz. J. Probab. Stat.* **18**, 69–102.

Cattrell, A.D., Srokosz, M., Moat, B.I. & Marsh, R. 2018 Can rogue waves be predicted using characteristic wave parameters? *J. Geophys. Res.* **123** (8), 5624–5636.

Cherneva, Z. & Guedes Soares, C. 2008 Non-linearity and non-stationarity of the new year abnormal wave. *Appl. Ocean Res.* **30** (3), 215–220.

Choi, Y., Lvov, Y.V. & Nazarenko, S. 2004 Probability densities and preservation of randomness in wave turbulence. *Phys. Lett.* A **332**, 230–238.

Choi, Y., Lvov, Y.V. & Nazarenko, S. 2005 Joint statistics of amplitudes and phases in wave turbulence. *Physica* D **201**, 121–149.

Christou, M. & Ewans, K. 2014 Field measurements of rogue water waves. *J. Phys. Oceanogr.* **9**, 2317–2335.

Cohen, L. 1989 Time–frequency distributions – a review. *Proc. IEEE* **77** (7), 941–981.

Cramér, H. & Leadbetter, M.R. 1967 *Stationary and Related Stochastic Processes*. John Wiley & Sons.

Das, S. & Nason, G.P. 2016 Measuring the degree of non-stationarity of a time series. *Stat* **5** (1), 295–305.

Davenport, W.B. & Root, W.L. 1987 *An Introduction to the Theory of Random Signals and Noise*. Wiley-IEEE Press.

Dean, R.G. & Dalrymple, R.A. 1984 *Water Wave Mechanics for Engineers and Scientists*. World Scientific.

Dematteis, G., Grafke, T., Onorato, M. & Vanden-Eijnden, E. 2019 Experimental evidence of hydrodynamic instantons: the universal route to rogue waves. *Phys. Rev.* X **91** (4), 041057.

Deodatis, G. & Shinozuka, M. 1988 Digital simulation of seismic ground motion using stochastic wave theory. In *Proceedings 9th World Conference on Earthquake Engineering*, vol. 2.

Dingemans, M.W. 1997 *Water Wave Propagation Over Uneven Bottoms*. World Scientific.

DONELAN, M.A., DRENNAN, W.M. & MAGNUSSON, A.K. 1996 Nonstationary analysis of the directional properties of propagating waves. *J. Phys. Oceanogr.* **26** (9), 1901–1914.

DUCROZET, G. & GOUIN, M. 2017 Influence of varying bathymetry in rogue wave occurrence within unidirectional and directional sea-states. *J. Ocean Engng Mar. Energy* **3** (4), 309–324.

DYSTHE, K., KROGSTAD, H.E. & MULLER, P. 2008 Oceanic rogue waves. *Annu. Rev. Fluid Mech.* **40**, 287–310.

EAGLESON, P.S. 1956 Properties of shoaling waves by theory and experiment. *Trans. Am. Geophys. Union* **37** (5), 565–572.

FAUKNER, D. 2002 Shipping safety: a matter of concern. In *Ingenia, The Royal Academy of Engineering, Marine Matters*, pp. 13–20.

FAULKNER, D. & BUCKLEY, W.H. 1997 Critical survival conditions for ship design. In *International Conference on Design and Operation for Abnormal Conditions, RINA*, vol. 6, pp. 1–25.

FEDELE, F., BRENNAN, J., DE LEON, S.P., DUDLEY, J. & DIAS, F. 2016 Real world ocean rogue waves explained without the modulational instability. *Sci. Rep.* **6**, 27715.

FLANDRIN, P 1989 *Time-Dependent Spectra for Non-Stationary Stochastic Processes*, pp. 69–124. Springer.

FORRISTALL, G.Z. 2000 Wave crest distributions: observations and second order theory. *J. Phys. Ocean.* **30**, 1931–1943.

FU, R., MA, Y., DONG, G. & PERLIN, M. 2021 A wavelet-based wave group detector and predictor of extreme events over unidirectional sloping bathymetry. *Ocean Engng* **229**, 108936.

GLUKHOVSKII, B.K. 1966 Investigation of sea wind waves (in Russian), Gidrometeoizdat. *Proc. Sea Climatology Conference*, pp. 51–71. Leningrad.

GODA, Y. 1983 A unified nonlinearity parameter of water waves. *Rept. Port Harbour Res. Inst.* **22** (3), 3–30.

GODA, Y. 2010 *Random Seas for Design of Maritime Structures*. World Scientific.

GRAMSTAD, O., ZENG, H., TRULSEN, K. & PEDERSEN, G.K. 2013 Freak waves in weakly nonlinear unidirectional wave trains over a sloping bottom in shallow water. *Phys. Fluids* **25** (12), 122103.

GUEDES SOARES, C., CHERNEVA, Z. & ANTAO, E.M. 2004 Steepness and asymmetry of the largest waves in storm sea states. *Ocean Engng* **31** (8–9), 1147–1167.

HASSELMANN, K. 1962 On the non-linear energy transfer in a gravity-wave spectrum. Part 1. General theory. *J. Fluid Mech.* **12** (4), 481–500.

HAVER, S. 2000 Evidences of the existence of freak waves. In *Rogue Waves 2000* (ed. M. Olagnon & G.A. Athanassoulis), pp. 129–140.

HAVER, S. & ANDERSEN, O.J. 2000 Freak waves: rare realizations of a typical population of typical realizations of a rare population? In *Proc. 10th Int. Offshore Polar Eng. Conf. Seattle*, vol. 3, pp. 123–130.

JANSSEN, P.A.E.M. 2014 On a random time series analysis valid for arbitrary spectral shape. *J. Fluid Mech.* **759**, 236–256.

JORDE, S. 2018 Kinematiken i bølger over en grunne. Master's thesis, University of Oslo.

KARMPADAKIS, I., SWAN, C. & CHRISTOU, M. 2020 Assessment of wave height distributions using an extensive field database. *Coast. Engng* **157**, 103630.

KHINTCHINE, A. 1934 Korrelationstheorie der stationären stochastischen prozesse. *Math. Ann.* **109** (1), 604–615.

KJELDSEN, S.P. 1984 Dangerous wave groups. *Nor. Marit. Res.* **12**, 4–16.

LAWRENCE, C., TRULSEN, K. & GRAMSTAD, O. 2021 Statistical properties of wave kinematics in long-crested irregular waves propagating over non-uniform bathymetry. *Phys. Fluids* **33** (4), 046601.

LÉ MÉHAUTE, B. 1976 *An Introduction to Hydrodynamics and Water Waves*. Springer.

LI, Y., DRAYCOTT, S., ADCOCK, T.A. & VAN DEN BREMER, T. 2021*a* Surface wavepackets subject to an abrupt depth change. Part 2. Experimental analysis. *J. Fluid Mech.* **915**, A72.

LI, Y., DRAYCOTT, S., ZHENG, Y., LIN, Z., ADCOCK, T.A.A. & VAN DEN BREMER, T.S. 2021*b* Why rogue waves occur atop abrupt depth transitions. *J. Fluid Mech.* **919**, R5.

LI, Y., ZHENG, Y., LIN, Z., ADCOCK, T.A. & VAN DEN BREMER, T. 2021*c* Surface wavepackets subject to an abrupt depth change. Part 1. Second-order theory. *J. Fluid Mech.* **915**, A71.

LINFOOT, B., STANSELL, P. & WOLFRAM, J. 2000 On the characteristics of storm waves. In *Proceedings of the International Offshore and Polar Engineering Conference*, vol. 3, pp. 74–83.

LONGUET-HIGGINS, M.S. 1952 On the statistical distribution of the heights of sea waves. *J. Mar. Res.* **11**, 245–265.

LONGUET-HIGGINS, M.S. 1963 The effect of non-linearities on statistical distributions in the theory of sea waves. *J. Fluid Mech.* **17**, 459–480.

LONGUET-HIGGINS, M.S. 1980 On the distribution of the heights of sea waves: some effects of nonlinearity and finite band width. *J. Geophys. Res.* **85** (C3), 1519–1523.

LOYNES, R.M. 1968 On the concept of the spectrum for non-stationary processes. *J. R. Stat. Soc.* B **30** (1), 1–30.

MA, Y.-X., MA, X.-Z. & DONG, G.-H. 2015 Variations of statistics for random waves propagating over a bar. *J. Mar. Sci. Technol.* **23** (6), 864–869.

MAJDA, A.J., MOORE, M.N.J. & QI, D. 2019 Statistical dynamical model to predict extreme events and anomalous features in shallow water waves with abrupt depth change. *Proc. Natl Acad. Sci. USA* **116** (10), 3982–3987.

MARTHINSEN, T. 1992 On the statistics of irregular second-order waves. *Rep. No.* RMS-11.

MASSEL, S.R. 2017 *Ocean Surface Waves: Their Physics and Prediction*, 3rd edn. World Scientific.

MENDES, S., SCOTTI, A. & STANSELL, P. 2021 On the physical constraints for the exceeding probability of deep water rogue waves. *Appl. Ocean Res.* **108**, 102402.

MICHE, R. 1944 Mouvements ondulatoires de la mer en profendeur constante ou decroissante forme limite de la houle lors de son deferlement. *Ann. Ponts Chaussees* **121**, 285–319.

MIDDLETON, D. 1996 *An Introduction to Statistical Communication Theory*. Wiley-IEEE.

MOORE, N.J., BOLLES, C.T., MAJDA, A.J. & QI, D. 2020 Anomalous waves triggered by abrupt depth changes: laboratory experiments and truncated KDV statistical mechanics. *J. Nonlinear Sci.* **30** (6), 3235–3263.

MORI, N. & YASUDA, T. 2002 A weakly non-Gaussian model of wave height distribution random wave train. *Ocean Engng* **29** (10), 1219–1231.

MYRHAUG, D. & KJELDSEN, S.P. 1986 Steepness and asymmetry of extreme waves and the highest waves in deep water. *Ocean Engng* **13** (6), 549–568.

NAESS, A. 1985 On the distribution of crest to trough wave heights. *Ocean Engng* **12** (3), 221–234.

NAGABHUSHANAM, K. & BHAGAVAN, C.S.K. 1969 A mean ergodic theorem for a class of non-stationary processes. *Indian J. Stat.* **31** (4), 421–424.

ONORATO, M., RESIDORI, S., BORTOLOZZO, U., MONTINA, A. & ARECCHI, F.T. 2013 Rogue waves and their generating mechanisms in different physical contexts. *Phys. Rep.* **528**, 47–89.

ONORATO, M. & SURET, P. 2016 Twenty years of progresses in oceanic rogue waves: the role played by weakly nonlinear models. *Nat. Hazards* **84**, 541–548.

PAPOULIS, A. 2002 *Probability, Random Variables and Stochastic Processes*, 4th edn. McGraw-Hill.

PENROSE, O. 1973 *Foundations of Statistical Mechanics*. Oxford University Press.

PHILLIPS, O.M. 1958 The equilibrium range in the spectrum of wind-generated waves. *J. Fluid Mech.* **4** (4), 426–434.

PIERSON, W.J. & MOSKOWITZ, L. 1964 A proposed spectral form for fully developed wind seas based on the similarity theory of S. A. Kitaigorodskii. *J. Geophys. Res.* **69** (24), 5181–5190.

RAUSTØL, A. 2014 Freake bølger over variabelt dyp. Master's thesis, University of Oslo.

RICE, S.O. 1945 Mathematical analysis of random noise. *Bell Syst. Tech. J.* **24** (1), 46–156.

RIPLEY, B.D. 1981 *Spatial Statistics*. Wiley-Interscience.

SALEHI, H. 1973 The spectrum and the law of large numbers for infinite-dimensional nonstationary stochastic processes. *J. Math. Anal. Appl.* **41** (3), 575–582.

SHERMAN, M. 2010 *Spatial Statistics and Spatio-Temporal Data: Covariance Functions and Directional Properties*. Wiley Series on Applied Probability. Wiley.

SHINOZUKA, M. & DEODATIS, G. 1988 Stochastic process models for earthquake ground motion. *Probab. Engng Mech.* **3** (3), 114–123.

SHINOZUKA, M. & JAN, C.-M. 1972 Digital simulation of random processes and its applications. *J. Sound Vib.* **25** (1), 111–128.

ST DENIS, M. & PIERSON, W.J. 1953 On the motions of ships in confused seas. *Trans. Soc. Nav. Archit.* **61**, 1–65.

STANSELL, P. 2004 Distribution of freak wave heights measured in the North Sea. *Appl. Ocean Res.* **26**, 35–48.

TAYFUN, M.A. 1980 Narrow-band nonlinear sea waves. *J. Geophys. Res.* **85**, 1548–1552.

TAYFUN, M.A. 1990 Distribution of large wave heights. *ASCE J. Waterway Port Coastal Ocean Engng* **116** (6), 686–707.

TAYFUN, M.A. 2006 Statistics of nonlinear wave crests and groups. *Ocean Engng* **33** (11), 1589–1622.

TAYFUN, M.A. 2008 Distributions of envelope and phase in wind waves. *J. Phys. Oceanogr.* **38** (12), 2784–2800.

TAYFUN, M.A. & ALKHALIDI, M.A. 2020 Distribution of sea-surface elevations in intermediate and shallow water depths. *Coastal Engng* **157**, 103651.

TAYFUN, M.A. & FEDELE, F. 2007 Wave-height distributions and nonlinear effects. *Ocean Engng* **34** (11), 1631–1649.

TOFFOLI, A., LEFEVRE, J.M., BITNER-GREGERSEN, E. & MONBALIU, J. 2005 Towards the identification of warning criteria: analysis of a ship accident database. *Appl. Ocean Res.* **27**, 281–291.

TRULSEN, K. 2018 Rogue waves in the ocean, the role of modulational instability, and abrupt changes of environmental conditions that can provoke non equilibrium wave dynamics. In *The Ocean in Motion: Circulation, Waves, Polar Oceanography* (ed. M.G. Velarde, R.Y. Tarakanov & A.V. Marchenko). Springer.

TRULSEN, K., RAUSTØL, A., JORDE, S. & RYE, L.B. 2020 Extreme wave statistics of long-crested irregular waves over a shoal. *J. Fluid Mech.* **882**, R2.

TRULSEN, K., ZENG, H. & GRAMSTAD, O. 2012 Laboratory evidence of freak waves provoked by non-uniform bathymetry. *Phys. Fluids* **24** (9), 097101.

TUNG, C.C. & HUANG, N.E. 1985 Peak and trough distributions of nonlinear waves. *Ocean Engng* **12**, 201–209.

VANDEVER, J.P., SIEGEL, E.M., BRUBAKER, J.M. & FRIEDRICHS, C.T. 2008 Influence of spectral width on wave height parameter estimates in coastal environments. *ASCE J. Waterway Port Coastal Ocean Engng* **134** (3), 187–194.

XU, J., LIU, S., LI, J. & JIA, W. 2021 Experimental study of wave height, crest, and trough distributions of directional irregular waves on a slope. *Ocean Engng* **242**, 110136.

ZAKHAROV, V.E. & OSTROVSKY, L.A. 2009 Modulation instability: the beginning. *Physica* D **238** (5), 540–548.

ZENG, H. & TRULSEN, K. 2012 Evolution of skewness and kurtosis of weakly nonlinear unidirectional waves over a sloping bottom. *Nat. Hazards Earth Syst. Sci.* **12** (3), 631–638.

ZHANG, J. & BENOIT, M. 2021 Wave–bottom interaction and extreme wave statistics due to shoaling and de-shoaling of irregular long-crested wave trains over steep seabed changes. *J. Fluid Mech.* **912**, A28.

ZHANG, J., BENOIT, M., KIMMOUN, O., CHABCHOUB, A. & HSU, H.-C. 2019 Statistics of extreme waves in coastal waters: large scale experiments and advanced numerical simulations. *Fluids* **4** (2), 99.

ZHENG, Y., LIN, Z., LI, Y., ADCOCK, T.A.A., LI, Y. & VAN DEN BREMER, T.S. 2020 Fully nonlinear simulations of unidirectional extreme waves provoked by strong depth transitions: the effect of slope. *Phys. Rev. Fluids* **5** (6), 064804.

ZOU, L., WANG, A., WANG, Z., PEI, Y. & LIU, X. 2019 Experimental study of freak waves due to three-dimensional island terrain in random wave. *Acta Oceanol. Sin.* **38** (6), 92–99.